Residual currents in a semi-enclosed bay of the Seto Inland Sea, Japan

Xinyu Guo
Center for Marine Environmental Studies, Ehime University, Matsuyama, Japan

Akira Futamura
Graduate School of Science and Engineering, Ehime University, Matsuyama, Japan

Hidetaka Takeoka
Center for Marine Environmental Studies, Ehime University, Matsuyama, Japan

Received 13 November 2003; revised 1 September 2004; accepted 27 September 2004; published 7 December 2004.

[1] On the basis of the Princeton Ocean Model, a robust diagnostic model is developed to calculate the residual currents in the Hiuchi-Nada, a semi-enclosed bay of the Seto Inland Sea. The input water temperature and salinity data are from six hydrographic surveys in 2002, and the model results in the summer show a clockwise eddy in the western part of the bay and an anticlockwise eddy in the eastern part. The magnitude of two eddies is ~10 cm/s. The modeled flow pattern is consistent with early observations derived from moored arrays. The two eddies are persistent throughout the summer because winds are usually weak and cannot influence their existence. The tide-induced residual currents are appreciable only in the close vicinity of the Kurushima Strait and Bisan Strait, the two straits connecting the bay to the other bays, and have little affect on the two eddies that are inside the bay. Thus the two density-driven eddies in the Hiuchi-Nada are the basic pattern of circulation in the summer. Using the calculated residual currents, we examined the intrusion route of waters from the Kurushima Strait and Bisan Strait with passive tracer experiments. The results show that the water in the Kurushima Strait intrudes into the bay mainly through the middle and bottom layers while the water in the Bisan Strait intrudes mainly through the surface layer. Furthermore, the tracer cannot reach the center of the anticlockwise eddy in the eastern part of the bay. This indicates that the eddy prevents water exchange between its center and outer edges and provides favorable conditions for the formation of oxygen-deficient waters in the central part of the eddy. *INDEX TERMS:* 4243 Oceanography: General: Marginal and semienclosed seas; 4255 Oceanography: General: Numerical modeling; 4512 Oceanography: Physical: Currents; *KEYWORDS:* residual current, diagnostic model, cold bottom water, eddy, Seto Inland Sea

Citation: Guo, X., A. Futamura, and H. Takeoka (2004), Residual currents in a semi-enclosed bay of the Seto Inland Sea, Japan, *J. Geophys. Res.*, *109*, C12008, doi:10.1029/2003JC002203.

1. Introduction

[2] Residual current is one of the fundamental issues in costal waters. Because of the presence of tidal current, observation of residual current in coastal waters is not easy. In this study, we present the residual current in the Hiuchi-Nada, a semi-enclosed bay of the Seto Inland Sea, Japan (Figure 1), calculated by a robust diagnostic model from temperature and salinity data. This bay has a size of about 50 km × 30 km and an average depth of about 20 m. Its western side is a narrow but deep strait (>50 m), Kurushima Strait, and its eastern side is a wide but shallow strait (<20 m), Bisan Strait.

[3] The predominant tidal constituent in the Seto Inland Sea is the lunar semidiurnal M_2 [*Yanagi and Higuchi*, 1981]. The tide propagates from the Pacific into the Seto Inland Sea through two channels, the Bungo Channel on the west and Kii Channel on the east, respectively. After entering through these channels, the tide propagates in opposite directions and converges at the Bisan Strait, inducing a standing wave in the Hiuchi-Nada [*Yanagi and Higuchi*, 1981]. The amplitude of the M_2 tide in the Hiuchi-Nada is over 1 m and produces strong tidal currents in the Kurushima Strait and Bisan Strait where the cross-sectional areas are small. The amplitude of M_2 tidal currents is 2.5 m/s in the Kurushima Strait and 0.95 m/s in the Bisan Strait [*Yanagi and Higuchi*, 1981]. The tidal current weakens rapidly as it enters the Hiuchi-Nada where the cross-sectional area expands. The weakest tidal currents appear in the eastern region of Hiuchi-Nada where the amplitude of the M_2 tidal current is around 0.1 m/s [*Yanagi and Higuchi*, 1981].

[4] An important environmental problem in the Hiuchi-Nada is the formation of a bottom oxygen-deficient water mass in the eastern region during the summer. This arises

0148-0227/04/2003JC002203$09.00

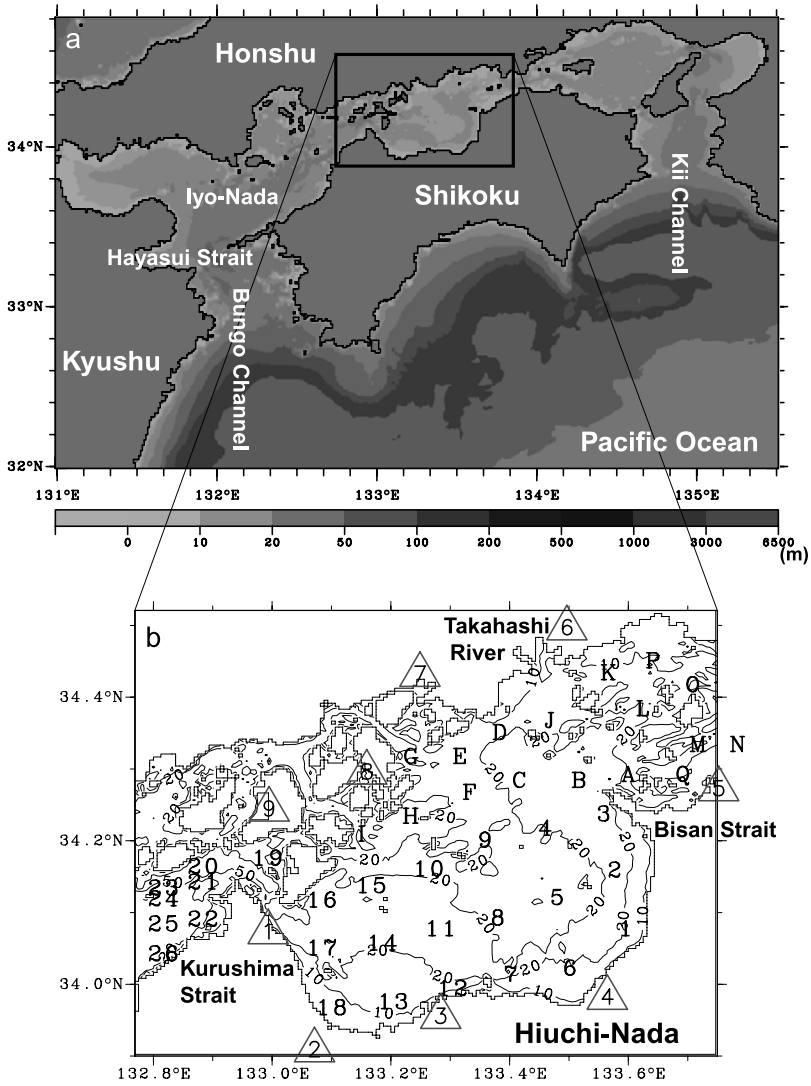

Figure 1. (a) Map of the Seto Inland Sea, Japan and (b) bathymetry of the Hiuchi-Nada, Kurushima Strait, and Bisan Strait. The contours in Figure 1b indicate water depth (m) and the numbers 1–26 and characters of A–Q denote CTD stations. The numbered triangles denote the stations where wind records are available from AMeDAS (Automated Meteorological Data Acquisition System), maintained by Japan Meteorological Agency. The names of station are IMABARI (1), TAMBARA (2), NIIHAMA (3), MISHIMA (4), TADOTSU (5), KASAOKA (6), FUKUYAMA (7), INNOSHIMA (8), and OMISHIMA (9).

from strong stratification in the eastern portion of Hiuchi-Nada, derived mostly from surface heating [*Takeoka*, 1985a]. Summer stratification prevents vertical supply of dissolved oxygen to the bottom layer. As degradation of organic materials consumes dissolved oxygen, an oxygen-deficient water mass forms in the bottom layer of the eastern region of the bay [*Ochi and Takeoka*, 1986]. Obviously, this explanation only considers the oxygen exchange in the vertical.

[5] The horizontal processes in the Hiuchi-Nada have not been well known. This is because the observations in the Hiuchi-Nada have mainly focused on the density structure and the biochemical parameters related to the oxygen consumption [*Ochi and Takeoka*, 1986; *Takeoka et al.*, 1991]. Knowledge of the residual current field is very limited. From 26 July to 8 August 1973 the 6th Regional Japan Coast Guard Headquarters carried out a survey of tidal current with 25-hour mooring current meters at 42 stations in the Hiuchi-Nada. As a byproduct, the residual current at a depth of 5 m was obtained (Figure 2). This is the only document on the residual current of this area. Because it offers no information on the current's vertical structure or its temporal variability, the circulation has not been linked to the formation of bottom oxygen-deficient water mass.

[6] As shown in Figure 1, the Hiuchi-Nada is located between two straits. The water exchange between the bay and the straits in the summer is suggested to be important to the density structure and nutrient supply in the bay [*Takeoka et al.*, 1991; *Takeoka*, 2002]. However, this process has not been well investigated. One reason is the existence of tidal fronts in the summer between the straits and the bay. In Figure 3, the distribution of $\log_{10}(H/u^3)$ is shown, where H

Figure 2. Distribution of residual currents observed with 25-hour mooring current meters from 26 July to 8 August 1973 by the Sixth Regional Japan Coast Guard Headquarters [after *Takeoka*, 1985b]. Short arrows are observed data and long arrows are inferred flow patterns.

is the water depth and u is the amplitude of the M_2 tidal current from the observed data [*Yanagi and Higuchi*, 1981]. *Simpson and Hunter* [1974] have shown that the tidal fronts should align along the contour of a critical value of this parameter. The critical value in the Seto Inland Sea is between 2.5 and 3.0 [*Yanagi and Okada*, 1993], and one of its corresponding tidal fronts has been observed between the Kurushima Strait and Hiuchi-Nada [*Yanagi and Yoshikawa*, 1987; *Takeoka*, 1990]. Usually the subtidal flow along fronts is 1 order of magnitude stronger than that across fronts [*Garrett and Loder*, 1981]. Therefore it is difficult to observe the inflow of strait water into the bay, which is across fronts, particularly with the presence of tidal currents.

[7] With the two above issues in mind, i.e., the three-dimensional structure of residual current in the Hiuchi-Nada and the inflow pathway of strait water into the bay, we carried out six hydrographic surveys in 2002 in the Hiuchi-Nada, Kurushima Strait, and Bisan Strait. A brief description of the observations is given in the next section. These observations are used in a robust diagnostic model (described in section 3) to obtain the residual current from each of the observed density fields (section 4). The vertical structure of two eddies obtained by the diagnostic model is examined in section 5. Through the release of passive tracer in the Kurushima Strait and Bisan Strait in the numerical model, we identified the inflow routes of strait water (section 6). Influences of tidal mixing on the calculated residual current, the response of the bay to winds in the summer, and tide-induced residual currents are discussed in section 7, followed by a short summary.

2. Observation and Results

[8] From the end of May to the beginning of December 2002, we carried out six hydrographic surveys at 43 stations in the Hiuchi-Nada, Kurushima Strait, and Bisan Strait (Figure 1). The dates and stations are listed in Table 1. Most surveys were completed in 2 or 3 days.

[9] The horizontal distributions of water temperature, salinity and density in the surface layer are depicted in Figure 4. At the end of May (Figure 4a), the lowest temperature was observed in the Kurushima Strait, the highest temperature in the eastern part of Hiuchi-Nada, and an intermediate temperature in the Bisan Strait and northern part of Hiuchi-Nada. This distribution pattern was unchanged in June and July (Figures 4b and 4c). In August (Figure 4d), the Bisan Strait and northern part of Hiuchi-Nada had similar high temperatures, but the eastern part of Hiuchi-Nada showed slightly decreased temperatures. In June, July, and August, the strongest horizontal gradients could be identified between the Kurushima Strait and Hiuchi-Nada. At the end of September (Figure 4e), the entire area had nearly the same temperature. At the end of November (Figure 4f), the coldest water was observed in the Bisan Strait and the warmest water in the Kurushima Strait.

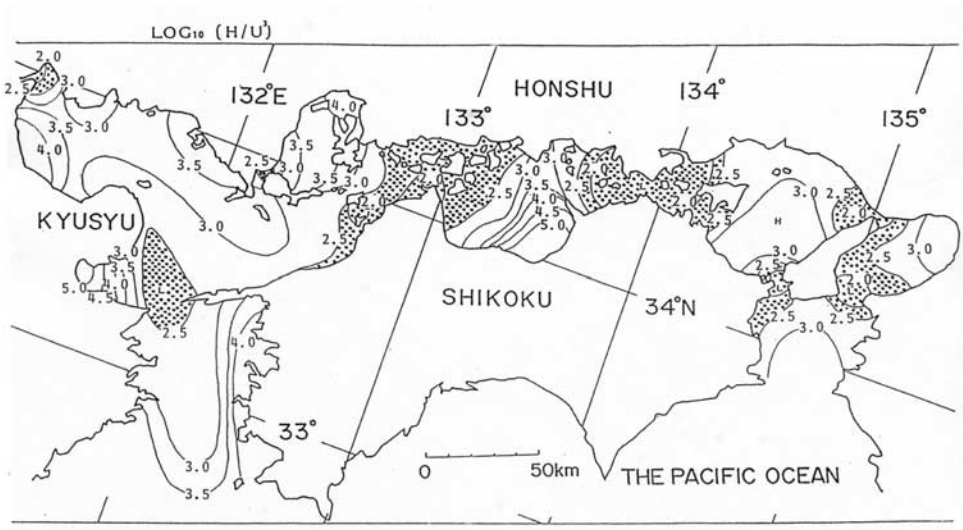

Figure 3. Distribution of $\log_{10}(H/u^3)$ in the Seto Inland Sea [after *Yanagi and Okada*, 1993]. Regions with values smaller than 2.5 are stippled.

Table 1. Dates and Stations of Observations in 2002[a]

Date	Stations
27/05–28/05	1, 2, 3, 4, 5, 6, 7, 8, 9, 10, 11, 12, 13, 14, 15, 16, 17, 18, 19, 20, 21, 22, 23, 24, 25, 26, A, B, C, D, E, F, G, H, J, K, L, M, N, O, P, Q
18/06–20/06	1, 2, 3, 4, 5, 6, 7, 8, 9, 10, 11, 12, 13, 14, 15, 16, 17, 18, 19, 20, 21, 22, 23, 24, 25, 26, A, B, C, D, E, F, G, H, I, J, K, L, M, N, O, P, Q
18/07–23/07	1, 2, 3, 4, 5, 6, 7, 8, 9, 10, 11, 12, 13, 14, 15, 16, 17, 18, 19, 20, 21, 22, 23, 24, 25, 26, A, B, C, D, E, F, G, H, I, J, K, L, M, N, O, P, Q
19/08–21/08	1, 2, 3, 4, 5, 6, 7, 8, 9, 10, 11, 12, 13, 14, 15, 16, 17, 18, 19, 20, 21, 22, 23, 24, 25, 26, A, B, C, D, E, F, G, H, I, J, K, L, M, N, O, P, Q
26/09–01/10	1, 2, 3, 4, 5, 6, 7, 8, 9, 10, 11, 12, 13, 14, 15, 16, 17, 18, 19, 20, 21, 22, 23, 24, 25, 26, A, B, C, D, E, F, G, H, I, J, K, L, M, N, O, P, Q
28/11–03/12	1, 2, 3, 4, 5, 6, 7, 8, 9, 10, 11, 12, 13, 14, 15, 16, 17, 18, 19, 20, 21, A, B, C, D, E, F, G, H, I, J, L, M, Q

[a]Dates given as dd/mm.

[10] The distribution of water temperature and its temporal variation (Figures 4a–4f) can be understood qualitatively by local heating or cooling. As suggested by Figure 3, the Kurushima Strait and Bisan Strait are well mixed throughout the year. In these straits, the surface heating or cooling affects the entire water column and the water temperature is inversely proportional to the water depth. With a nearly uniform heat flux input in the two straits [*Tawara*, 1986], the shallow Bisan Strait is more easily warmed or cooled than the deep Kurushima Strait. In the Seto Inland Sea, the warming and cooling start in March and September, respectively [*Ishizaki and Saito*, 1978]. Therefore we observed a higher temperature in the Bisan Strait than in the Kurushima Strait from May to August, the same temperature in the two straits at the end of September, and a lower temperature in the Bisan Strait at the end of November. On the other hand, water column stratification makes heat accumulate in the surface layer and reflects the highest surface temperature in the eastern region of Hiuchi-Nada in May, June, and July. The low surface temperature in the eastern region of Hiuchi-Nada in August may be caused by a relatively strong wind during the observation period (Figure 5), accompanied by the passage of a typhoon south of Shikoku 1 day before our observation.

[11] There are two low-salinity areas in the surface layer from May to September (Figures 4g–4l). One is at the northern part of Bisan Strait. The other is at the southwestern part of Hiuchi-Nada. They are likely direct results of runoff from Takahashi River, a major river located at the northern coast of Bisan Strait (Figure 1), and some small rivers along the southwestern coast of Hiuchi-Nada.

[12] With the lowest temperature and highest salinity, the water in the Kurushima Strait was the heaviest from May to September (Figures 4m–4r); with the lowest salinity and increasing temperature, the water in the Bisan Strait gradually became the lightest. Being the warmest, the surface water in the eastern part of Hiuchi-Nada was always among the lightest. As shown later, the bottom water in the eastern part of Hiuchi-Nada that had the lowest water temperature and highest salinity was also the heaviest water mass in this area in June, July, and August.

[13] In order to examine stratification in the entire water column, the potential energy anomaly is calculated (Figure 6). This variable has been used as an indicator of vertical stratification in many studies [*Simpson et al.*, 1977; *Hill et al.*, 1997; *Bisagni*, 1999]. It is defined as

$$\mathrm{PEA} = \frac{1}{h}\int_{-h}^{0} (\rho - \bar{\rho}) g z dz, \tag{1}$$

where h is the water depth, ρ is the water density, g is gravity, z is vertical coordinate with origin at sea surface and positive upward, and $\bar{\rho} = \frac{1}{h}\int_{-h}^{0} \rho dz$. PEA in (1) has units of Joule/m^3 and is the potential energy anomaly per unit volume. The larger the PEA is the stronger the stratification.

[14] In May, the largest value of PEA (>80 Joule/m^3) appeared in the southeastern part of Hiuchi-Nada and the smallest value in the Kurushima Strait and Bisan Strait. This pattern was maintained in June and July with small increase of the maximum value of PEA, suggesting the full development of stratification by May continuing on through

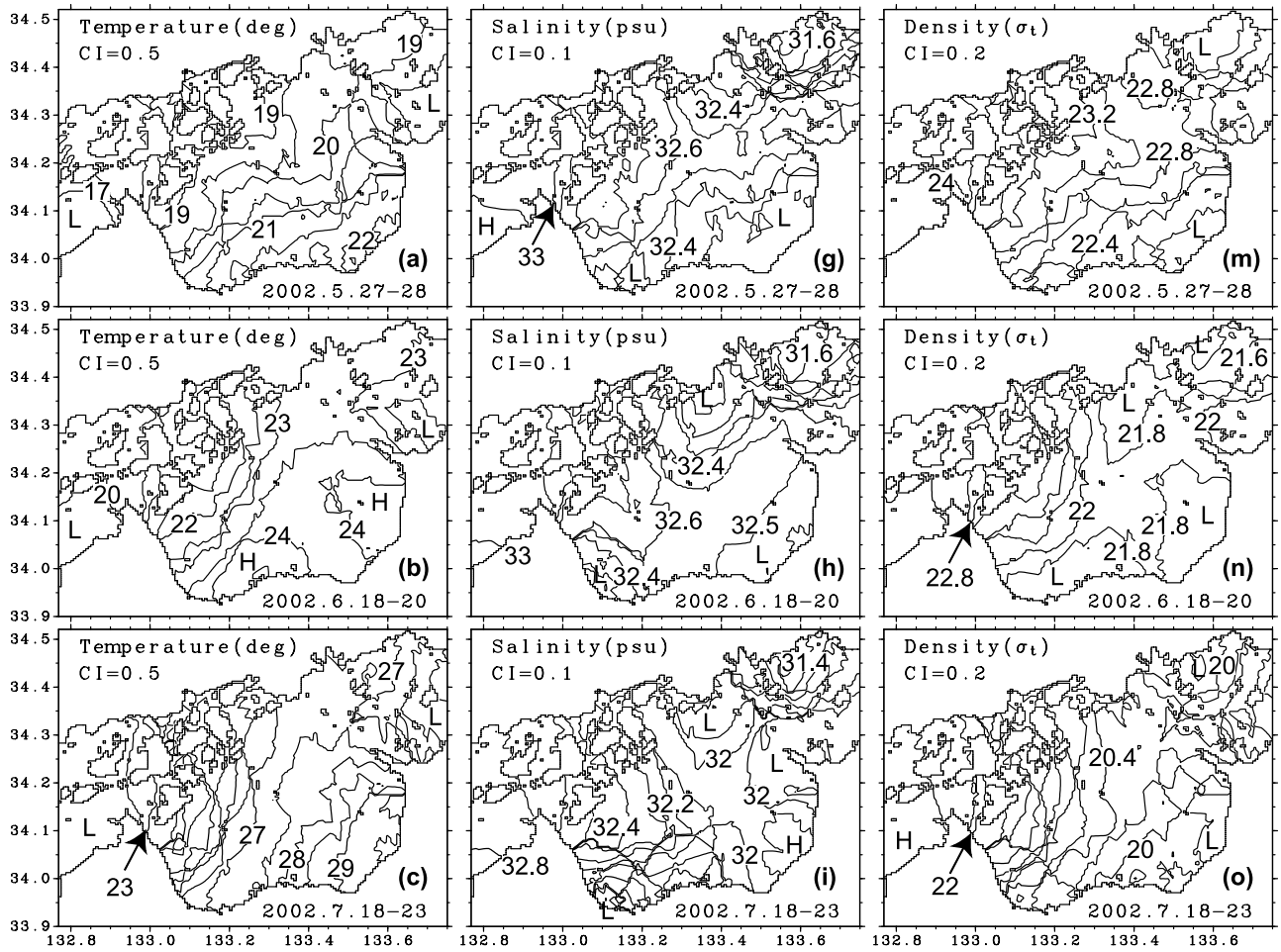

Figure 4. (a–f) Water temperature, (g–l) salinity, and (m–r) density at surface layer observed in 2002. Observation dates are plotted in each panel. H denotes high value, and L denotes low value. An objective interpolation scheme has been used to calculate the value at each grid point. The weight of each data used in the interpolation is calculated by $\exp(-r/r0)$ where r is the distance (in degrees) between CTD station and grid point and $r0$ is a given value ($0.1°\sim0.3°$) which is variable to ensure at least three CTD data to be involved in the interpolation.

June and July. However, the area with the largest PEA (>80 Joule/m^3) shifted slightly northward between May and July. In August, the stratification weakened because of the strong wind event during the observation (Figure 5). In September and November the entire area was vertically mixed due to surface cooling and wind.

3. Robust Diagnostic Model

[15] Residual currents in the Seto Inland Sea have three main components: density-driven, wind-driven, and tide-induced currents. The barotropic throughflow is very weak in the Seto Inland Sea [*Fujiwara and Higo*, 1986] and is omitted in this study.

[16] Because of the strong effects of tidal mixing near the two straits, a diagnostic model [*Sarkisyan and Ivanov*, 1971; *Holland and Hirschman*, 1972] rather than geostrophic method is used to calculate residual currents in this study. *Holland and Hirschman* [1972] show that the calculated currents tend to be sensitive to the input density field that is fixed in the diagnostic model. To overcome this problem, *Sarmiento and Bryan* [1982] propose a robust diagnostic model that solves the conservation equations for temperature and salinity in a prognostic way. The observed temperature and salinity data are included in the conservation equations with an additional damping term. Compared to a typical diagnostic model [*Sarkisyan and Ivanov*, 1971; *Holland and Hirschman*, 1972], the robust diagnostic model is more resistant to minor inconsistencies in the input density data and produces a smooth current field and a consistent density field [*Sarmiento and Bryan*, 1982].

[17] To avoid inconsistencies in the input density data is difficult in coastal waters. Tidal currents always induce inconsistencies in the density field obtained by a snapshot observation. Objective interpolations, which produce the input density field from limited observed data, also introduce inconsistencies. Therefore a robust diagnostic model rather than a diagnostic model is the choice for calculating residual currents in coastal waters.

[18] One of the community ocean models for coastal waters, the Princeton Ocean Model (POM [*Blumberg and Mellor*, 1987; *Mellor*, 1998]), is adopted to be the base of

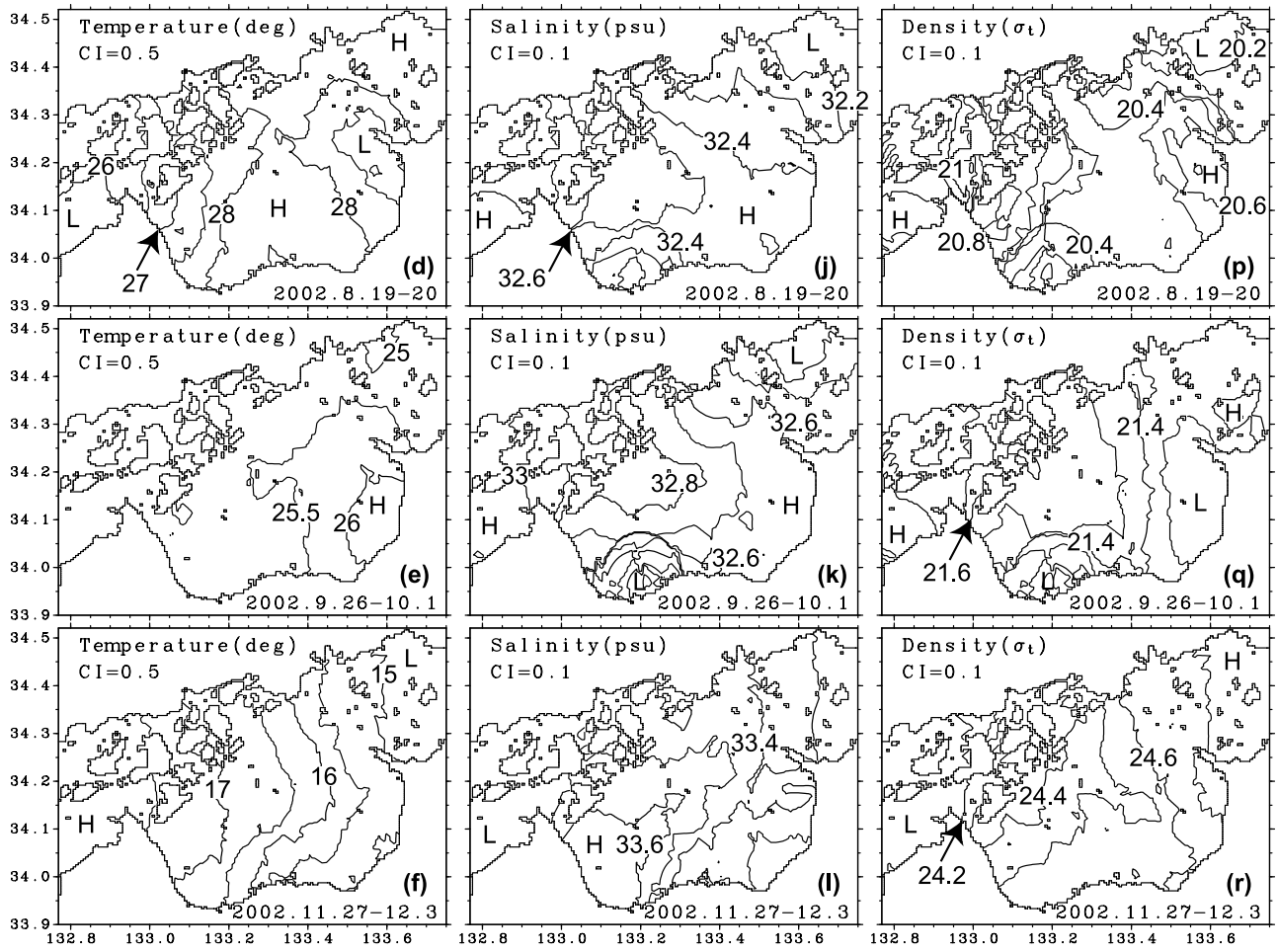

Figure 4. (continued)

the robust diagnostic model. The original POM is modified through the introduction of a damping term in the equations for temperature and salinity as follows:

$$\frac{\partial T}{\partial t}+u\frac{\partial T}{\partial x}+v\frac{\partial T}{\partial x}+w\frac{\partial T}{\partial z}=\frac{\partial}{\partial x}\left(A_H\frac{\partial T}{\partial x}\right)+\frac{\partial}{\partial y}\left(A_H\frac{\partial T}{\partial y}\right)+\frac{\partial}{\partial z}\left(A_V\frac{\partial T}{\partial z}\right)+\gamma(T^*-T), \quad (2)$$

where T is temperature or salinity, u, v, w are the three components of velocity, A_H and A_V are horizontal and vertical diffusivities, respectively, and T^* is observed temperature or salinity; γ is a parameter controlling the role of observed data T^*.

[19] The model domain and topography are shown in Figure 1b. The horizontal resolution is roughly 500 m (1/160° in the zonal direction and 1/240° in the meridional direction). The relatively high resolution in the horizontal is necessary to represent the narrow channels around the Kurushima Strait (Figure 1). There are 21 sigma-levels in the vertical (Table 2) with finer grid interval near surface and bottom. The bottom stresses are calculated using a

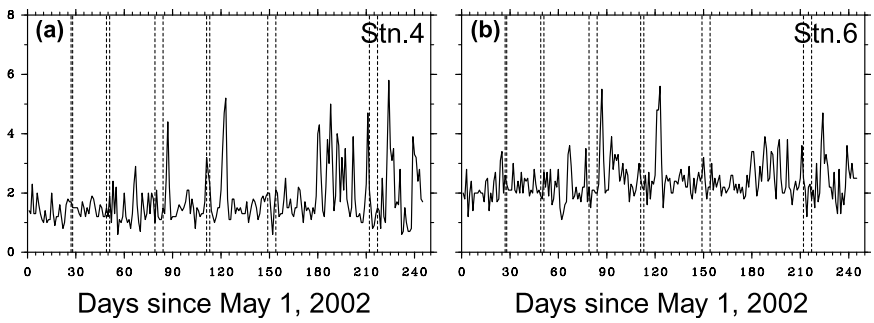

Figure 5. Time series of daily mean wind speed (m/s) records at stations 4 and 6 from May to the end of 2002. Data at the other stations (see Figure 1 for positions of all stations) show a similar temporal variation. The time between two broken lines are the periods of observations.

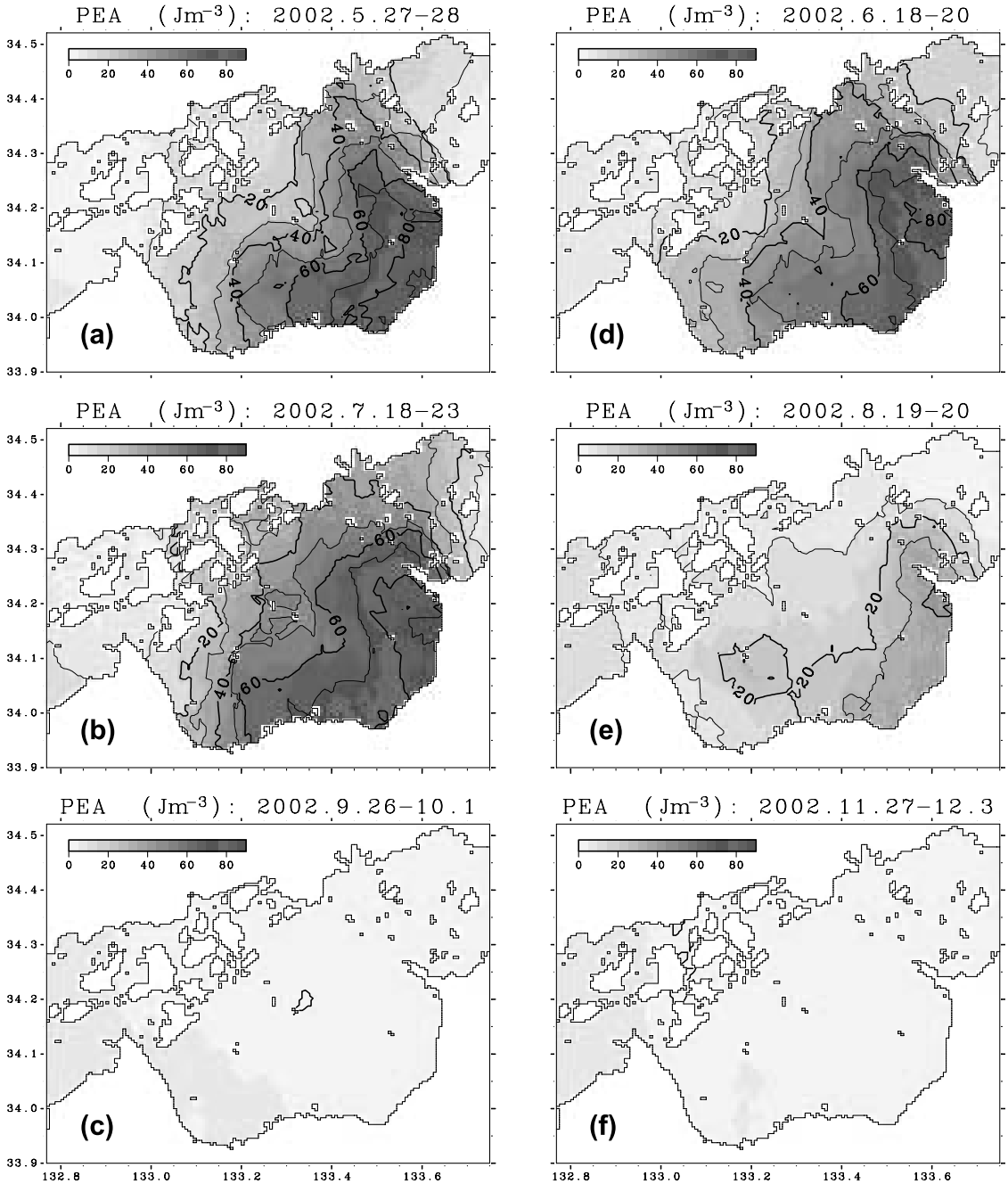

Figure 6. Distribution of potential energy anomaly per unit volume. See equation (1) for the definition.

quadratic friction law, and the bottom drag coefficient is calculated by the embedded formula in the POM [*Mellor*, 1998]. The time step is 2 s for the external mode and 60 s for the internal mode.

[20] To ensure that the current related to the pressure gradient error is small, the topography data are smoothed with the embedded subroutine SLPMIN in the POM to satisfy the criteria given by *Mellor et al.* [1994],

$$\frac{|H_{i+1} - H_i|}{(H_{i+1} + H_i)} \leq \alpha, \tag{3}$$

where H_{i+1} and H_i are the depths at two adjacent grids, α is a slope factor (=0.2).

[21] Physically, the pressure gradient error should be small in this study. This is because the pressure gradient error tends to be large only when water depth variations combine with strong stratification [*Mellor et al.*, 1994]. In our study area, the water depth varies greatly near or in the straits (Figure 1) where the water is always homogeneous (Figure 6). On the other hand, the regions with strong stratification (Figure 6) have small gradients of depth (Figure 1). Estimation of velocity induced by the pressure gradient error in a manner similar to *Beckmann and Haidvogel* [1993] and *Mellor et al.* [1998] shows that the maximum velocity with the vertical profiles of density obtained from six surveys occurs around the Kurushima Strait and is less than 2 cm/s. Beyond the Kurushima

Table 2. Values of Sigma-Coordinate

Layer	Sigma-Coordinate
1	0.000
2	−0.009
3	−0.018
4	−0.036
5	−0.071
6	−0.143
7	−0.214
8	−0.286
9	−0.357
10	−0.429
11	−0.500
12	−0.571
13	−0.643
14	−0.714
15	−0.786
16	−0.857
17	−0.929
18	−0.964
19	−0.982
20	−0.991
21	−1.000

Strait, the magnitude of velocity is less than 1 cm/s. Therefore the effects of pressure gradient error can be negligible in this study.

[22] We do not directly include tidal currents in diagnostic calculations but consider their mixing effects by relating eddy viscosities and diffusivities to tidal currents. Usually, tidal currents are stronger than residual currents by 1 order of magnitude. Direct inclusion of tidal currents in the calculations of residual currents could induce residual currents to be of the same order of magnitude as the calculation error of tidal currents. Furthermore, separation of density-driven, wind-driven, and tide-induced components of residual currents becomes impossible.

[23] The Mellor-Yamada (MY) turbulence closure model [*Mellor and Yamada*, 1982] embedded in the POM is used to estimate vertical eddy viscosity and diffusivity dependent on tidal currents. *Simpson et al.* [1996] show that the MY closure model can simulate well their observed turbulent dissipation in the Irish Sea where the tidal currents have an amplitude from 0.45 m/s to 1.0 m/s. *Burchard et al.* [1998] compare the performance of MY and $k-\varepsilon$ turbulence models and show that both models can predict well the data obtained by *Simpson et al.* [1996]. *Wijesekera et al.* [2003] compare three turbulent closure schemes (MY closure, $k-\varepsilon$ closure, and K-Profile Parameterization) and show that all three turbulent models produce similar features in the circulation and qualitatively similar eddy diffusivities and eddy viscosities.

[24] Several prognostic calculations were carried out in advance to obtain the vertical eddy viscosity and diffusivity related to tidal currents. The M_2 tidal current was imposed along the western and eastern boundaries of the model domain where the harmonic constants were obtained from a tidal model of the entire Seto Inland Sea [*Harai et al.*, 2001]. The observed temperature and salinity fields (Figure 4) were used as the initial values. The calculations also produce horizontal eddy viscosity on the basis of the Smagorinsky formula [*Mellor*, 1998] with a proportionality parameter of 0.1, and horizontal eddy diffusivity with a given inverse Prandtl number (=0.5).

[25] As shown by *Simpson et al.* [1996], *Stacey et al.* [1999], and *Lu et al.* [2000], the vertical eddy viscosity varies temporally with tidal phase. The horizontal eddy viscosity has similar temporal variations as well. The combined effects of temporally varying vertical or horizontal eddy viscosities and vertical or horizontal shears of tidal currents could induce residual currents, but they are parts of the tide-induced residual current. In our diagnostic calculations, tidally averaged vertical and horizontal eddy viscosities and diffusivities were used.

[26] Figure 7 presents horizontal distributions of A_H and A_V at three depths. Eddy viscosities have similar distributions to these two parameters. In the Kurushima Strait and Bisan Strait, large vertical ($0.01\sim0.1$ m^2/s) and horizontal ($10\sim100$ m^2/s) eddy diffusivities are obtained. In the eastern part of bay, small vertical ($\sim10^{-5}$ m^2/s) and horizontal (~0.1 m^2/s) eddy diffusivities are obtained. Relatively large vertical eddy diffusivity is obtained near the bottom (Figure 7c).

[27] We have no direct observations to verify the calculated vertical and horizontal eddy viscosities (Figure 7), particularly the large values in the Kurushima Strait. However, in a partially stratified channel in northern San Francisco Bay, where the amplitude of tidal current is 0.7–0.9 m/s, *Stacey et al.* [1999] show an observed vertical eddy viscosity ranging from 0.005 m^2/s to over 0.02 m^2/s, with the maximum values occurring near the bottom. *Lu et al.* [2000] also present an observed vertical eddy viscosity ranging from 0.001 m^2/s to over 0.3 m^2/s in a tidal channel where the amplitude of the tidal current was about 1.0 m/s. Thus, considering the stronger M_2 tidal current ($\sim$2.5 m/s) in the Kurushima Strait, the estimates of vertical eddy viscosity (Figure 7) seem reasonable. As for the horizontal eddy diffusivity, *Hayami and Unoki* [1970] suggest a value of 1000 m^2/s for the reproduction of salinity distribution in the Seto Inland Sea in a one-dimensional model. When density-driven currents are considered, this value can be reduced by 30 to 50% [*Murakami et al.*, 1985], which is on the same order as those obtained in the two straits (Figure 7).

[28] An important issue of the robust diagnostic model is the determination of γ, which is a free parameter. Physically, it controls the role of observed data in (2). *Sarmiento and Bryan* [1982] show that the ratio of the damping term $\gamma(T^*-T)$ to the horizontal advection term in (2) is $\gamma L^*/V^*$, where V^* is a scale velocity and L^* is a scale length. A small γ weakens the effects of damping term, and the advection term dominates the conservation equation. In this case, the model approaches a prognostic model. On the other hand, a large γ makes the model approach a pure diagnostic model ($T=T^*$) in which the advection effect is weak. In the calculations of the Atlantic, *Sarmiento and Bryan* [1982] use a depth-dependent γ that ranges from 1/50 day^{-1} to 1/250 day^{-1}. In the calculations of the Pacific, *Fujio and Imasato* [1991] use a latitude-dependent γ that ranges from 1/50 day^{-1} to zero. From $\gamma L^*/V^*$, we know that in the application with small horizontal scale like the Hiuchi-Nada, a large γ is needed to keep the same ratio of damping term to the advection term as that in the application with large horizontal scale such as the Atlantic or the Pacific, if the scale velocities are of the same order.

[29] We carried out a series of calculations to examine the response of model results to γ. With a decrease of γ, the

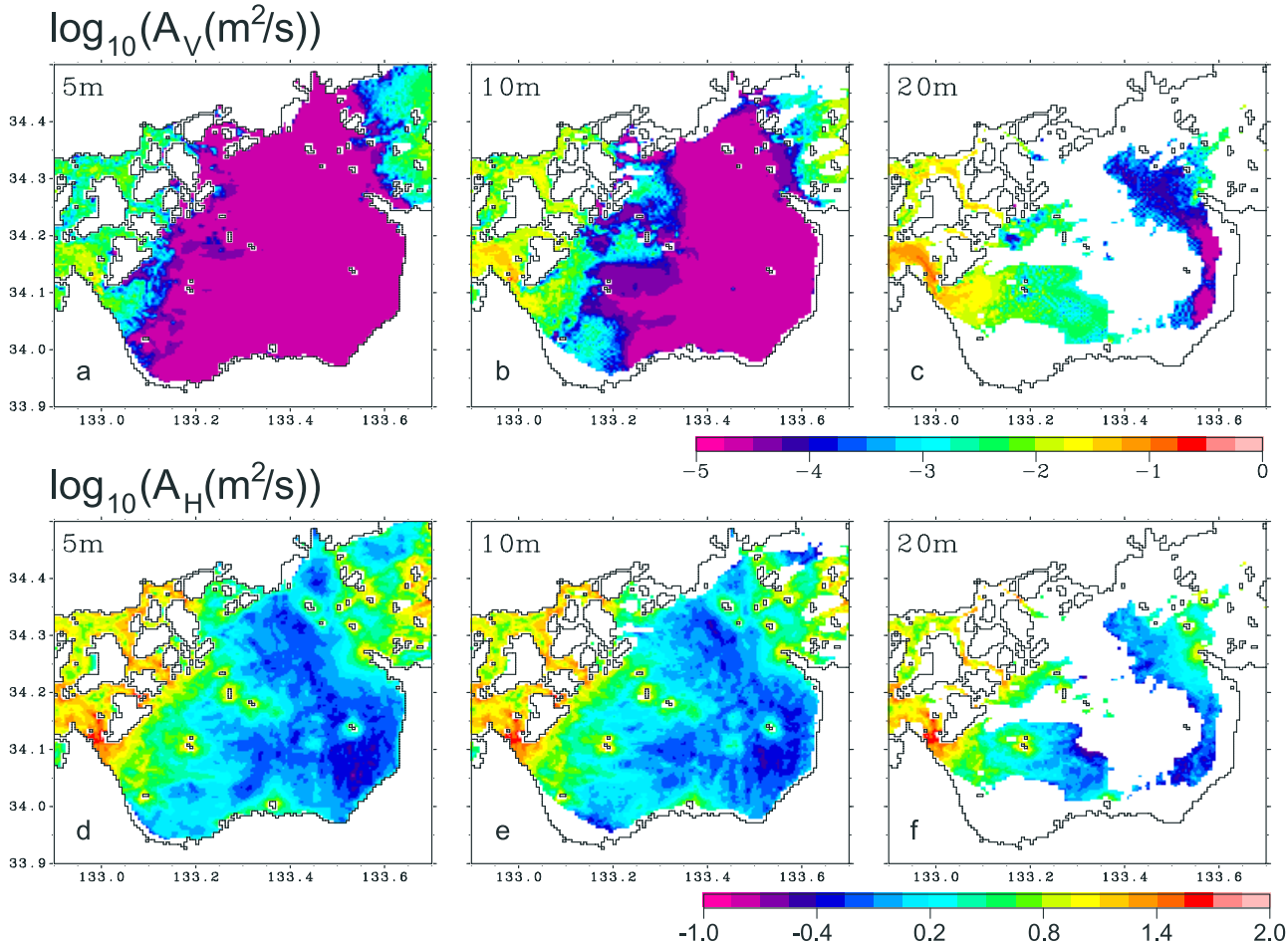

Figure 7. Horizontal distribution of tidally averaged (a–c) vertical and (d–f) horizontal eddy diffusivities at 5, 10, and 20 m from the calculation for July with tide.

calculated temperature and salinity deviates gradually from the initial values (Figure 8). From the viewpoint of diagnosing the velocity from hydrographic data, a larger γ is preferable. The difference between the calculated currents and observations (Figure 2) reaches a minimum as γ equals to 0.5 day^{-1}. Because there is little difference in the calculated currents as γ varies from 1.0 to 0.2 day^{-1}, we set γ to 1 day^{-1}. We notice that the same value of γ has been used in the calculations of the East China Sea [*Yanagi and Takahashi*, 1993] and the Tokyo Bay, Japan [*Guo and Yanagi*, 1996].

[30] The initial temperature and salinity in the diagnostic model are the same as the observed water temperature and salinity fields (Figure 4). The initial velocity and sea level is zero. The western and eastern boundaries are treated as wall in the diagnostic calculations. As the calculations started, the pressure gradient from the initial temperature and salinity produced currents that in turn are used to adjust the distribution of temperature and salinity. At the same time, the damping term in (2) constrains the calculated temperature and salinity to the observations. After 10 days, the model approaches a steady state where the mean velocity over the entire model domain has been stable and the calculated currents and density field are dynamically consistent with each other. The wind stresses were not initially included, and their impact will be discussed in section 7.2. Therefore the currents from the above calculations are density-driven flows.

4. Current Patterns

[31] In May, a large clockwise eddy in the southern part of Hiuchi-Nada dominates the surface layer (Figure 9a), while a southward current in the central part dominates the middle layer (Figure 9b). An anticlockwise eddy forms in the northeastern part, which is stronger in the middle layer than in the surface layer (Figures 9a and 9b). The current in the bottom layer (Figure 9c) is weak. In June, a clockwise eddy dominates the surface layer in the western part of Hiuchi-Nada (Figure 9d). In the eastern part, an anticlockwise eddy develops, and it is stronger in the surface layer than in the middle layer (Figure 9e). The southward current in the central part of the middle layer remains and extends to the surface layer. In the bottom layer (Figure 9f), a northward current is found along the eastern coast of Hiuchi-Nada. In July (Figures 10a–10c) and August (Figures 10d and 10e), the current pattern is similar to that in June, but the current itself intensifies in July and weakens in August. In September and November (Figure 11), the current patterns are completely different from those in June, July, and August and show rather incoherent distributions.

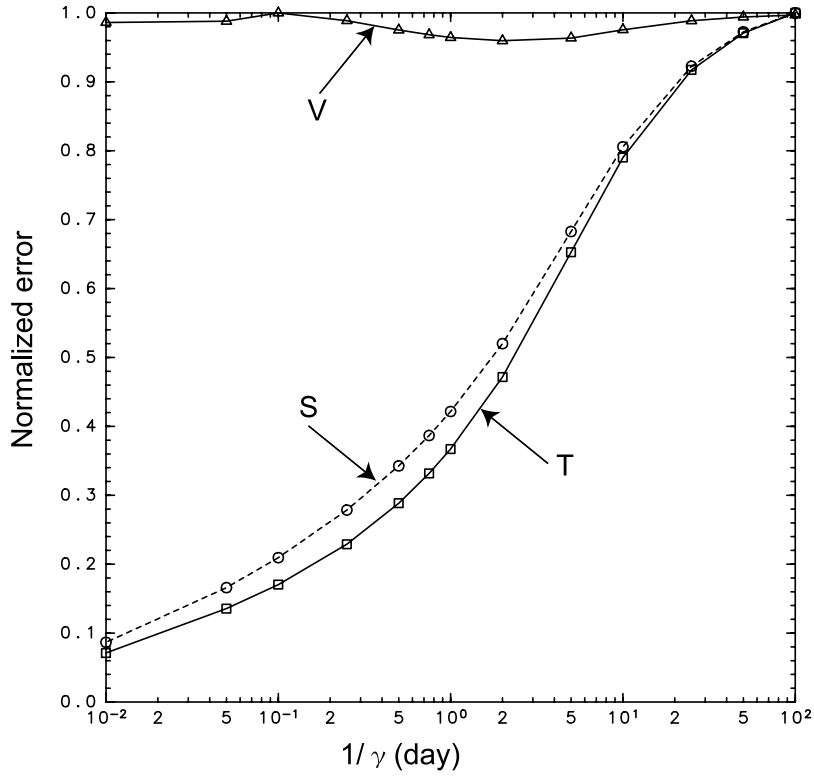

Figure 8. Model response to the change of γ. Errors for temperature (T) and salinity (S) are defined as the average of $|T_{initial} - T|$ at all grid points, where $T_{initial}$ is the initial value of temperature or salinity, and T is the calculated one; error for velocity (V) is defined as the average of $\sqrt{(u_{obs}-u)^2+(v_{obs}-v)^2}$ at 42 stations shown in Figure 2, where $u_{obs}\}$ and v_{obs} are the eastward and northward components of observed currents (Figure 2), u and v are calculated ones at the corresponding grid point. All three errors are normalized by the corresponding maximum values, 0.68°, 0.09 psu, and 9 cm/s for temperature, salinity, and velocity, respectively. All the results are from the July calculations.

[32] The calculated current pattern in the surface layer in July (Figures 10a and 10b) can be compared with the observed currents (Figure 2) because wind forcing during the period of current observations was very weak, and the tide-induced residual current is restricted to the vicinity of the Kurushima Strait and Bisan Strait (shown later). In the eastern part of Hiuchi-Nada, the anticlockwise eddy with a speed of 10 cm/s (Figures 10a and 10b) is consistent with observations (Figure 2). Over the western part of the Hiuchi-Nada, observations show a northward current southeast of the Kurushima Strait and a northeastward current northeast of the Kurushima Strait. Lack of data between these two locations makes it difficult to link them as a northward current. Model results suggest they are part of a northward current between the Kurushima Strait and Hiuchi-Nada. Therefore, in the summer the basic flow pattern in the Hiuchi-Nada consists of a clockwise eddy in the western part and an anticlockwise eddy in the eastern part.

5. Vertical Structure of Two Eddies

[33] Figure 10 shows that the two eddies have different vertical structure. The clockwise eddy in the western part concentrates in the surface layer, while the anticlockwise eddy in the eastern part intrudes into the middle layer. Further examination of the vertical structure of the two eddies can be effected with the distributions of temperature, salinity, density, and northward current along a section across the two eddies (Figure 12; see Figure 10f for section's position). In the western part of Hiuchi-Nada, a tidal front with horizontal density gradient of 1 kg m^{-3}/10 km can be identified (Figure 12c). The northward current accompanying this front has a strong vertical shear and its speed at the surface reaches ~10 cm/s (Figure 12d). Dynamically, this northward current is the geostrophic flow associated with the density structure of the tidal front [*Garrett and Loder*, 1981]. Because the northward current accompanying the tidal front is the major part of the clockwise eddy in the western part of the bay, the tidal front formed in the summer is therefore the major cause for the formation of the clockwise eddy. The tidal front can be maintained only in the summer. When the cooling starts, the clockwise eddy on the western part disappears (Figure 11).

[34] In the eastern part of Hiuchi-Nada, the presence of cold bottom water is evident and results in a temperature difference of more than 6° between surface and bottom. Combined with the salinity difference (~0.4 psu), the vertical gradient of density is about 1 kg m^{-3}/10 m. The anticlockwise eddy exists above the cold (also dense) bottom water with small vertical shear. This eddy is also geostrophically balanced by looking at the sea level distribution in Figure 10. Dynamically, it is possible for a

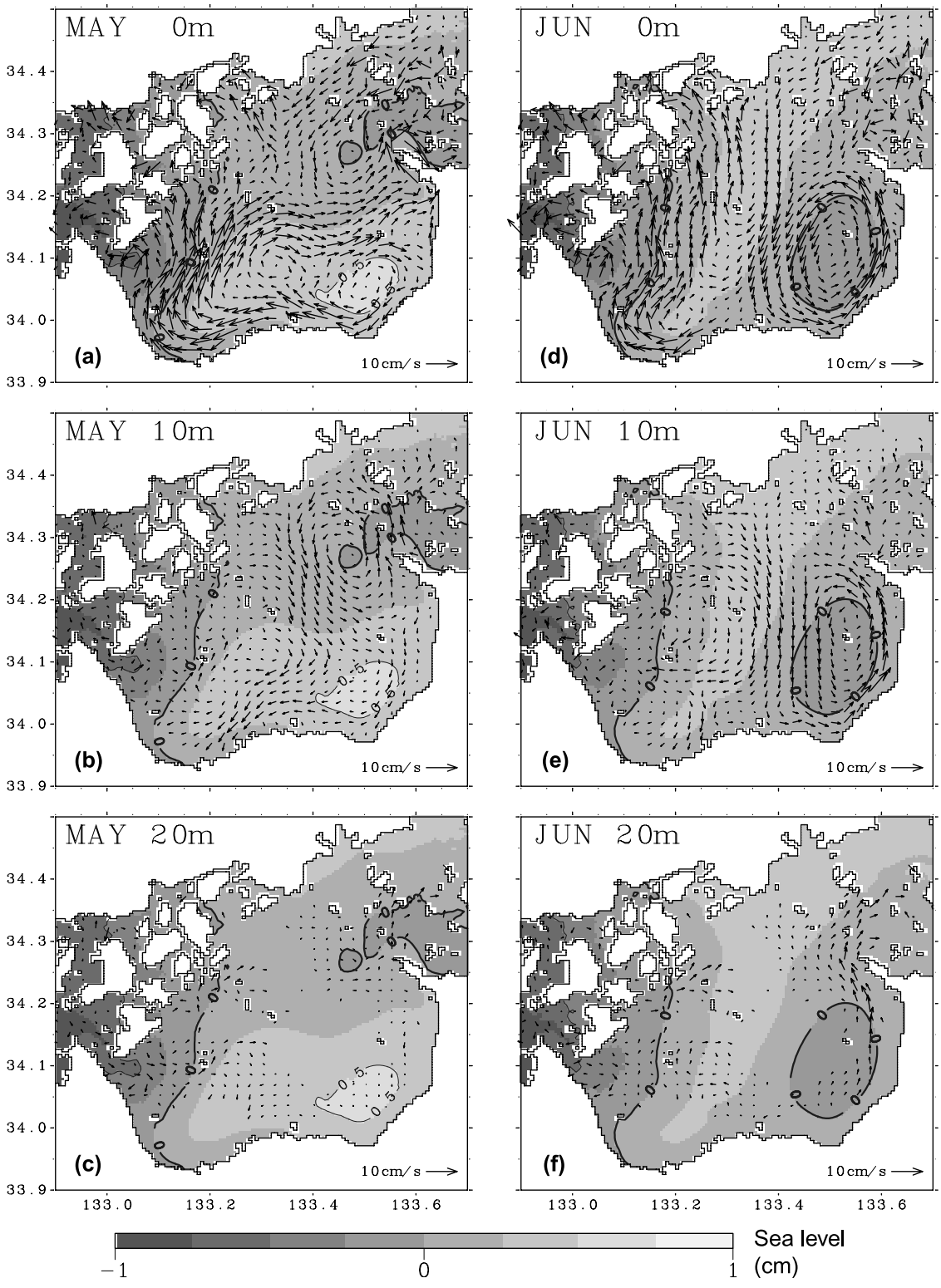

Figure 9. Horizontal distribution of residual currents at 0, 10, and 20 m in May and June. Sea level distributions are also shown in all panels as a reference.

clockwise circulation to develop in the dense (cold) bottom dome water while the water above it remains at rest. However, this situation is difficult to maintain in coastal waters because the bottom layer spins down to rest in a few days due to bottom friction, and an anticlockwise circulation finally develops above the dense (cold) bottom dome water [*Hill*, 1996]. This mechanism has been used to explain the existence of a cyclonic gyre in the summer in the surface layer of the western Irish Sea where cold bottom water exists [*Hill et al.*, 1997]. The same mechanism could also be

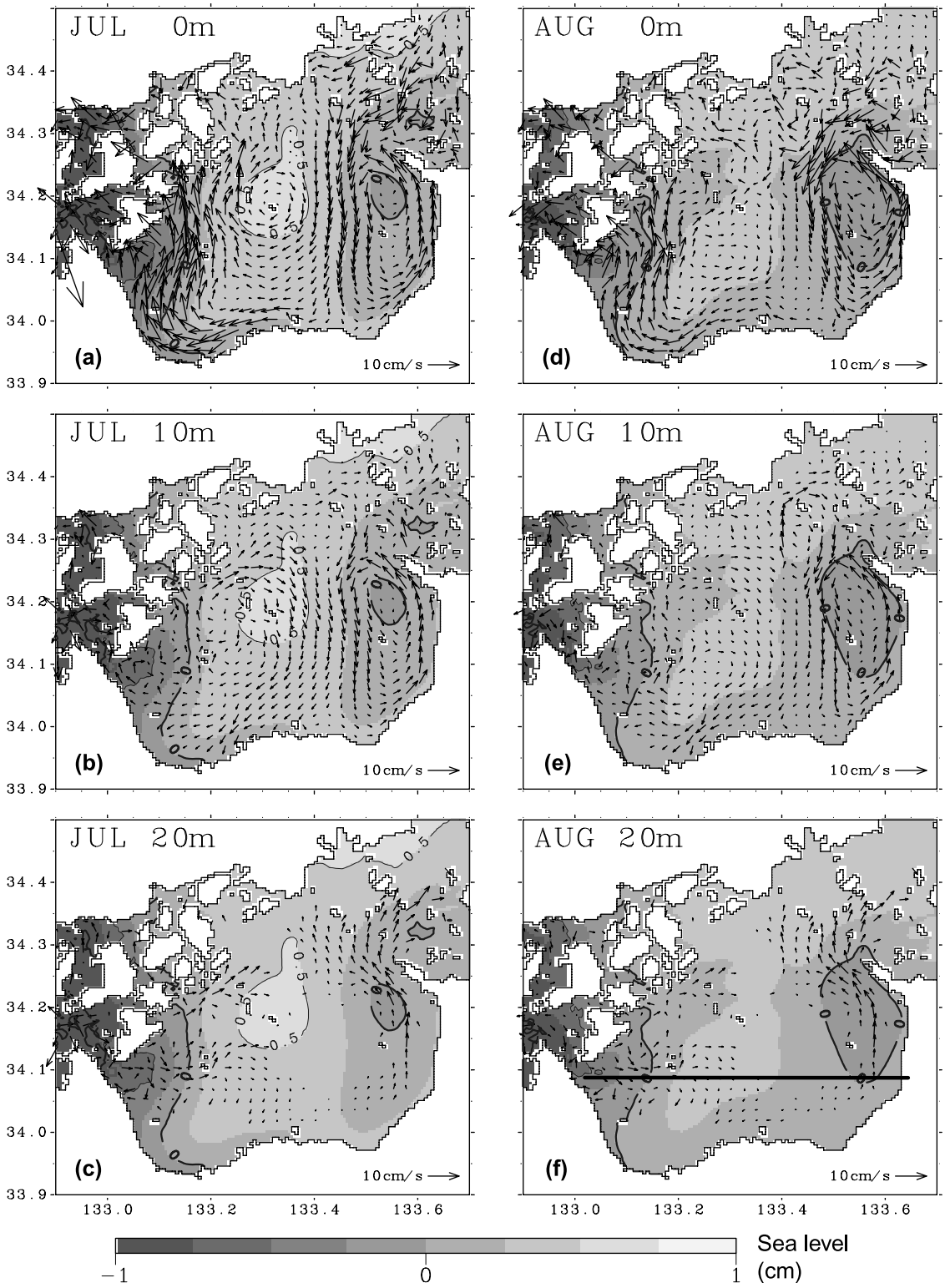

Figure 10. The same as Figure 9 but for July and August. The zonal line in Figure 10f represents the position of a section, along which the distribution of temperature, salinity, density, and northward velocity are shown in Figure 12.

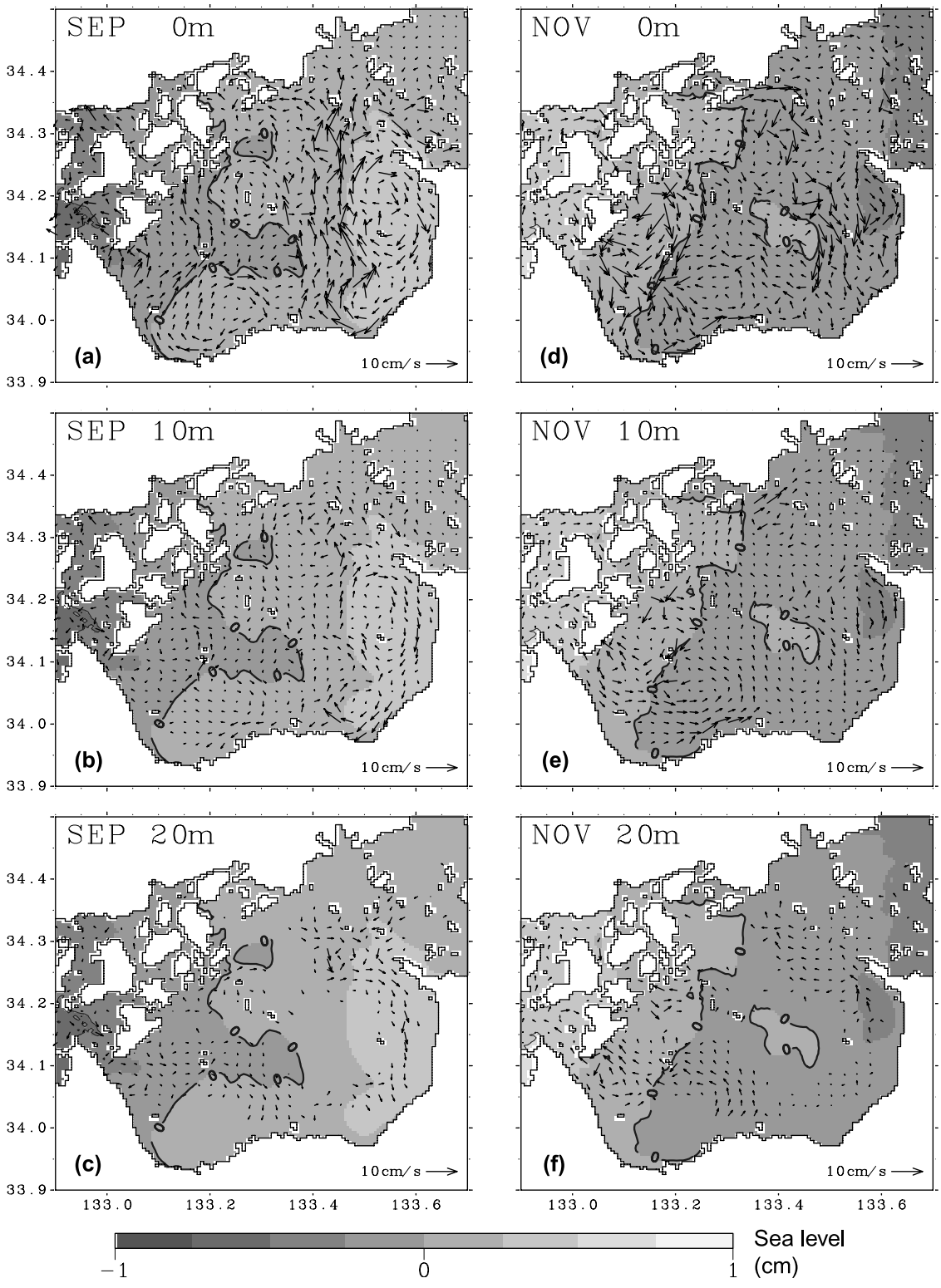

Figure 11. The same as Figure 9 but for September and November.

responsible for the presence of the anticlockwise eddy in the eastern part of Hiuchi-Nada.

6. Intrusion Routes of Strait Water

[35] To clarify the pathways of strait water into the Hiuchi-Nada, we continually release passive tracers with a value of 100 in the Kurushima Strait (tracer A, 132.95–130.05E, 34.0–34.4N, see Figure 1b for location) and Bisan Strait (tracer B, 133.6–133.75E, 34.25–34.5N), respectively. Both passive tracers are controlled by the same equation as the temperature, but without the γ term. The currents shown in Figures 9–11 and the horizontal and vertical eddy diffusivities (Figure 7) are adopted in the tracer calculations.

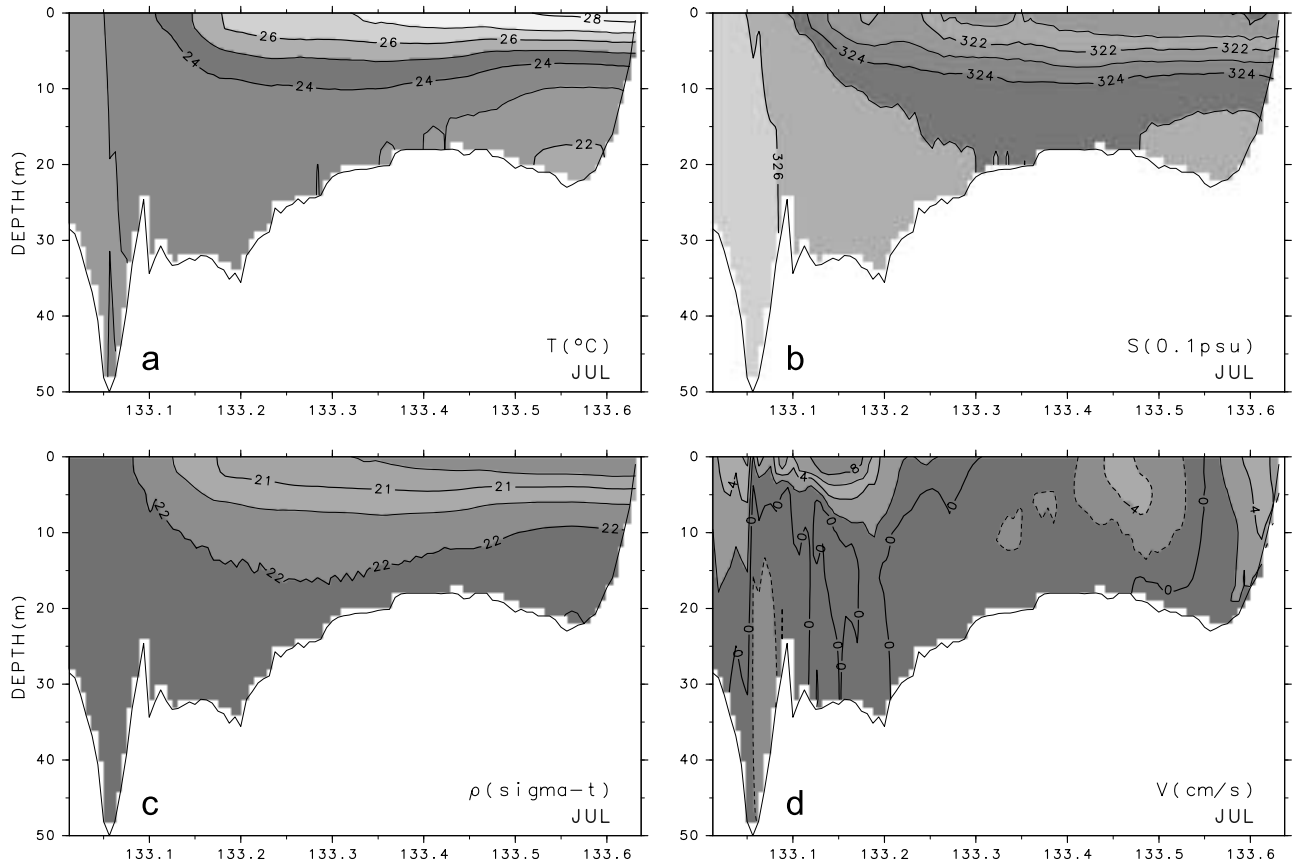

Figure 12. Vertical distribution of (a) temperature, (b) salinity, (c) density, and (d) northward velocity along a zonal section shown in Figure 10f. Results are from July calculations.

[36] The distributions of tracers, 30 days after their release in the Kurushima Strait and Bisan Strait, are shown in Figures 13 and 14, respectively. From May to August, the tracer A cannot enter the Hiuchi-Nada through the surface layer because of the northward current along the tidal front east of the Kurushima Strait. In the middle and bottom layers, the tracer A reaches as far as the central part of Hiuchi-Nada, particularly in July and August. Figures 10c and 10f show a flow from the Kurushima Strait to the Hiuchi-Nada in the bottom layer, which must be responsible for the bottom intrusion of Kurushima Strait water. In the middle layer, we do not observe a clear current toward the Hiuchi-Nada in Figures 10b and 10e. Therefore the strong vertical mixing near the bottom (Figure 7c) could be responsible for the tracer in the middle layer in July and August. In November, breakdown of the tidal front enables the tracer A to enter the Hiuchi-Nada through the surface layer, together with the current along the southern coast of Hiuchi-Nada (Figure 11d).

[37] The tracer B shows a different intrusion route (Figure 14). A major intrusion occurs in the surface layer. In May, the intrusion is weak and most of the tracer stays in the northern part of Hiuchi-Nada. From June to August, the intrusion becomes gradually strong. After reaching the southern coast of Hiuchi-Nada, the tracer B in the surface layer is caught by the anticlockwise eddy in the eastern part of Hiuchi-Nada, except in July when portions of the tracer are transported westward and reach the tidal front area east of the Kurushima Strait. In September and November, the intrusion becomes weak.

[38] In summer, the water of the Kurushima Strait enters the Hiuchi-Nada through the bottom layer while that of the Bisan Strait enters through the surface layer. The counter-intrusion route of the water from two straits can be understood from the density structure between the straits and the Hiuchi-Nada. As shown in Figure 4, with strong tidal mixing in the two straits, the deepest water column makes the water in the Kurushima Strait the heaviest in summer, while the shallowest water column makes the water in the Bisan Strait the lightest. Therefore the water from the Kurushima Strait intrudes mainly from the bottom layer, while that from the Bisan Strait intrudes from the surface layer.

[39] In July and August, most of the tracer B trapped by the anticlockwise eddy in the eastern part of Hiuchi-Nada stays only in the outer side of the eddy and does not reach the center of the eddy (Figure 14). This indicates the anticlockwise eddy isolates the water in its center from the water in its outer edges. This isolation could contribute to the formation of oxygen-deficient water mass in the center of the eddy in summer because the concentration of oxygen is usually high outside the cold bottom water. An example is given in Figure 15, in which the temperature and concentration of dissolved oxygen (DO) at 10 m and 20 m from an observation in July 2003 are shown. At 10 m, a cold water mass can be identified in the eastern part of the

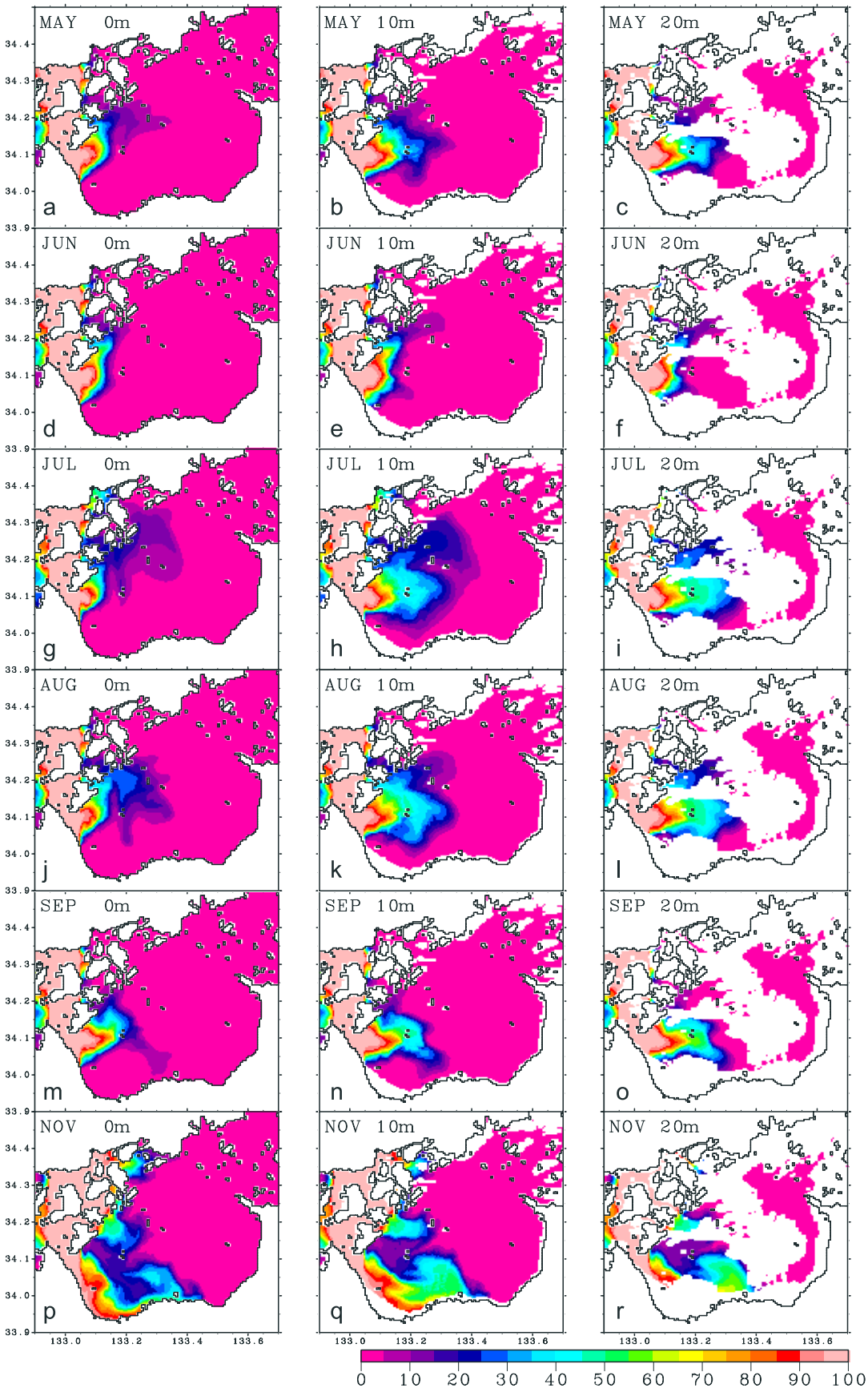

Figure 13. Horizontal distribution of tracer concentration at 0, 10, and 20 m, 30 days after being released in the Kurushima Strait.

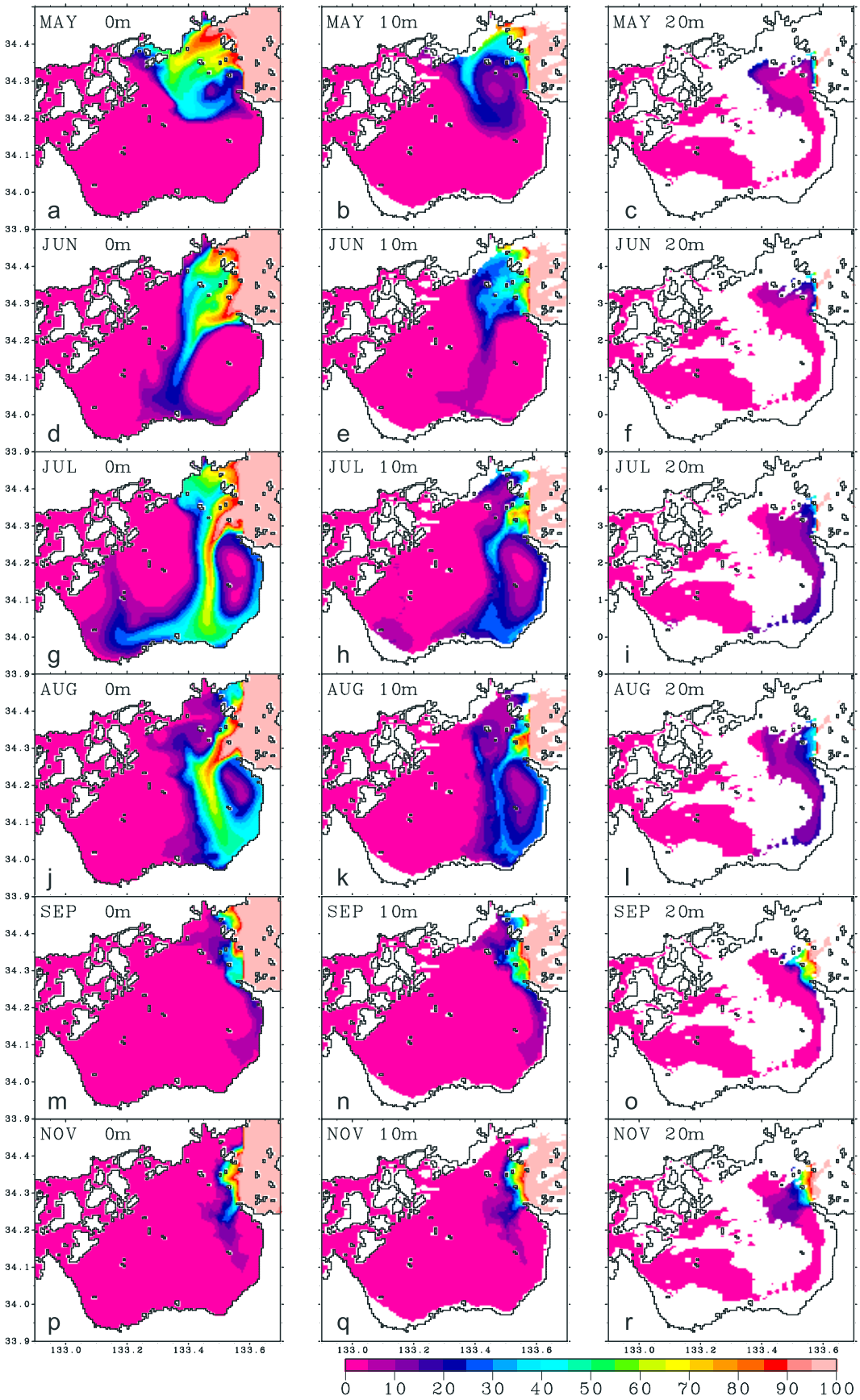

Figure 14. Horizontal distribution of tracer concentration at 0, 10, and 20 m, 30 days after being released in the Bisan Strait.

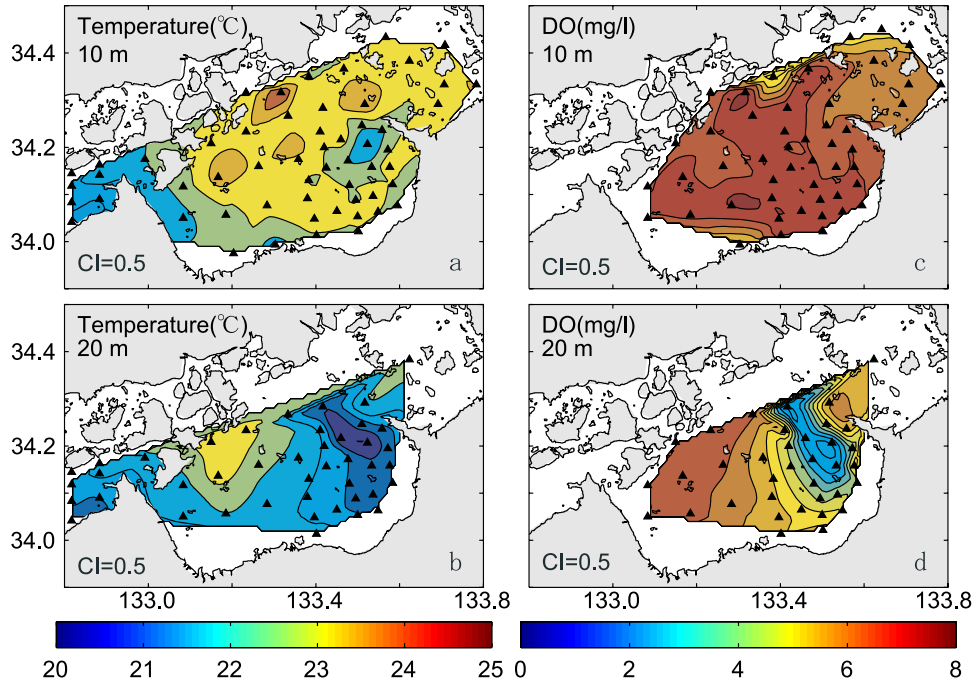

Figure 15. (a, b) Horizontal distribution of temperature and (c, d) concentration of dissolved oxygen at 10 and 20 m, from an observation in July 2003. The black triangles denote the observation stations.

bay but the concentration of DO in the cold water is not lower than the surrounding waters. At 20 m, a cold water mass can also be identified and the concentration of DO is lower than the surrounding areas; that is, the area with low concentration of DO coincides with the area with low temperature. Outside the bottom cold water, high concentration of DO was observed.

[40] The observed distribution of DO cannot be explained only by the isolation of the eddy. In addition to the horizontal processes, the vertical supply of oxygen and the biological processes related to the supply and consumption of oxygen also affect concentrations of DO. However, isolation of the eddy (Figure 14), at least, hinders the horizontal supply of oxygen to the center of the eddy.

7. Discussions

7.1. Effects of Tidal Mixing on Density-Driven Current

[41] To demonstrate the effects of tidal mixing on density-driven currents, as well as to examine the sensitivity of density-driven currents to the vertical eddy viscosity, we carried out some calculations in which the vertical and horizontal eddy viscosities were also calculated by the MY turbulent closure model and Smagorinsky formula, respectively, but without tide. An example of vertical and horizontal eddy viscosities given by these new calculations is shown in Figure 16. Compared to Figure 7, the new vertical and horizontal eddy viscosities are much smaller than those related to tidal currents, in particular in the Kurushima Strait and Bisan Strait.

[42] From Figure 17, we see that smaller viscosity is favorable for the development of density-driven currents in straits. Comparing Figure 17 to Figures 9–11, the basic flow patterns in each month are the same but the intensity of the two eddies becomes stronger in the cases without effects of tidal mixing (Figure 17). The largest difference is in the Kurushima Strait, where strong currents develop in the cases without effects of tidal mixing. This demonstrates the importance of tidal effects in calculations of the residual current in the Seto Inland Sea, where the strong tidal current in the straits produces large viscosity that weakens the residual current in the straits.

7.2. Effect of Wind

[43] In addition to density-driven currents, wind-driven currents are also important for the residual current in coastal waters. As shown in Figure 5, summer winds over the Hiuchi-Nada are usually weak. Although there are some spatial variations from station to station, the mean wind speed in the summer can be taken as 2 m/s. After September, winds become strong with several energetic pulses.

[44] To examine the effects of wind on the two eddies in the Hiuchi-Nada during the summer, winds from the east, west, north, and south with speeds of 2 m/s were added in the July calculation. The wind stress, τ, prescribed in the model is calculated with $\tau = \rho_a C_d U_a^2$, where ρ_a(= 1.2 kg/m^3) is air density, C_d (= 1.3 × 10^{-3}) is drag coefficient, and U_a is wind speed. The currents obtained in the surface layer respond directly to the imposed wind and are different from the results without wind forcing (Figure 10a). However, in the layer just underneath, for example at 5 m (Figure 18), little difference can be found in the calculated currents by the cases with and without wind forcing. The clockwise eddy in the western side and the anticlockwise eddy in the eastern side are hardly affected by the summer wind. This suggests that the basic circulation pattern of the two eddies persists throughout the summer. In fact, the calculated current pattern in August (Figure 10) implies that the two

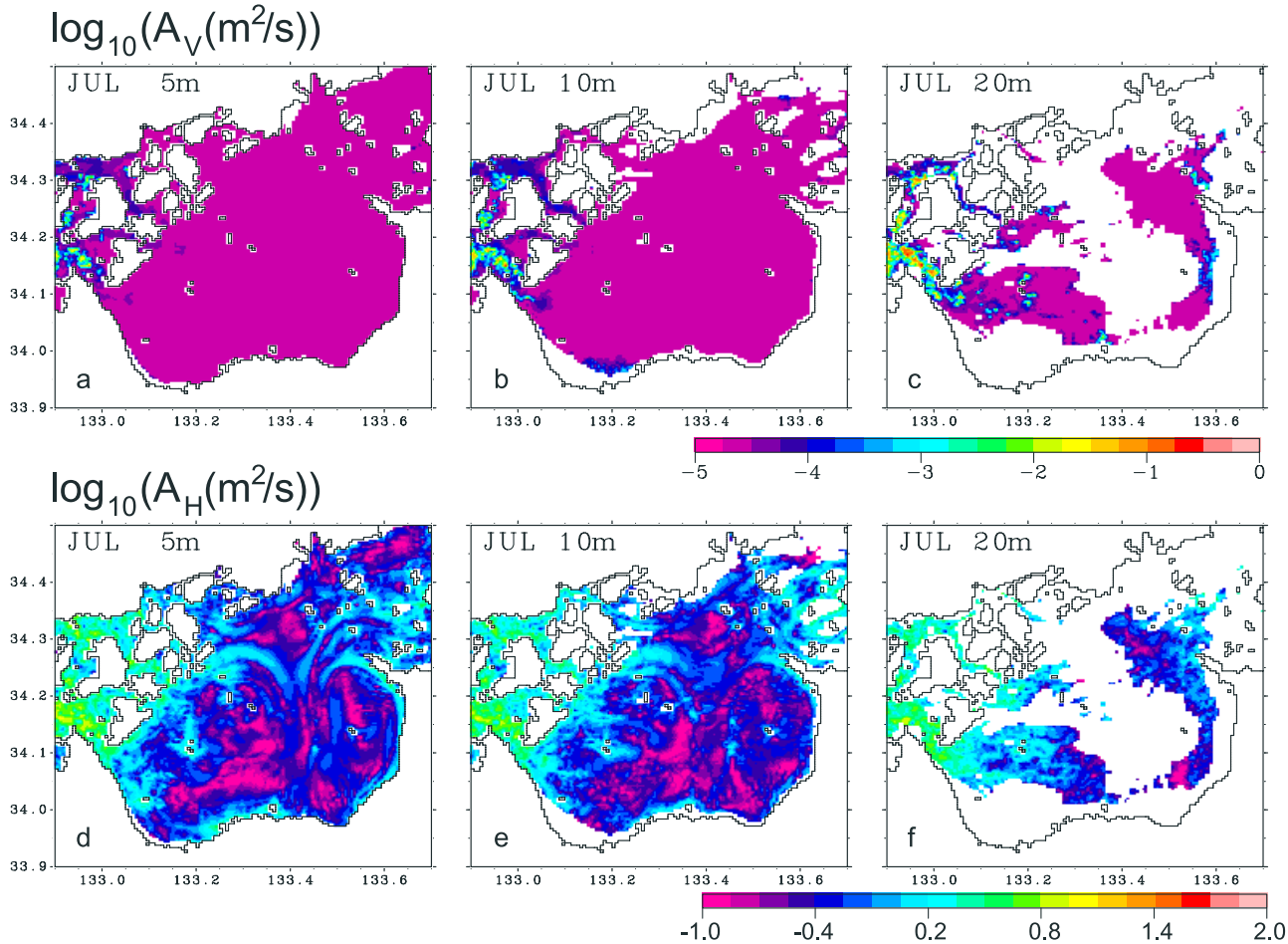

Figure 16. Horizontal distribution of (a–c) vertical and (d–f) horizontal eddy viscosities at 5, 10, and 20 m from the July calculation without tide.

eddies can exist even after a strong wind event that mixed the surface layer.

7.3. Tide-Induced Residual Current

[45] Tide-induced residual currents resulting from nonlinear effects of tidal currents are the third component of the residual flow in our study area. To obtain the tide-induced residual currents, the model with spatially constant temperature and salinity was driven by the M_2 tidal current in a manner the same as that in the prognostic model described in section 2. Harmonic analysis of model results gives the distribution of tide-induced residual currents (Figure 19). Only in the vicinity of the two straits, tide-induced residual currents are strong. Near the Kurushima Strait, tide-induced residual currents form an anticlockwise eddy that slightly weakens with depth. In the Hiuchi-Nada, tide-induced residual currents are weaker than 2 cm/s. Thus they do not affect the fate of the two eddies in the Hiuchi-Nada in the summer.

[46] With inclusion of tide-induced residual currents, we carried out passive tracer experiments again. The tracer released in the Kurushima strait (Figure 20) is greatly influenced by tide-induced residual currents but the tracer released in the Bisan Strait is little affected (not shown here). As tide-induced residual currents are added to density-driven currents in the tracer experiments, much more tracer is transported from the Kurushima Strait to the Hiuchi-Nada (Figure 20). After 30 days, it reaches the central area of Hiuchi-Nada or the eastern area of Hiuchi-Nada. However, the intrusion of water from the Kurushima Strait is still stronger in the middle and bottom layers than in the surface layer. This is because the tide-induced residual current near the Kurushima Strait has little variation in the vertical (Figure 19). Therefore, tide-induced residual currents do not affect the intrusion pathway of waters from the two straits into the Hiuchi-Nada.

8. Summary

[47] This study clarifies two issues, the three-dimensional structure of residual currents in the Hiuchi-Nada and the intrusion pathway of waters from the Kurushima Strait and Bisan Strait into the Hiuchi-Nada. The main results are summarized in Figure 21.

[48] With a robust diagnostic model, we obtain the density-driven current in the Hiuchi-Nada from hydrographic data and find the existence of two eddies in the summer, which is consistent with early observations derived from moored arrays. One is a clockwise eddy in the western part, associated with the tidal front between the Kurushima

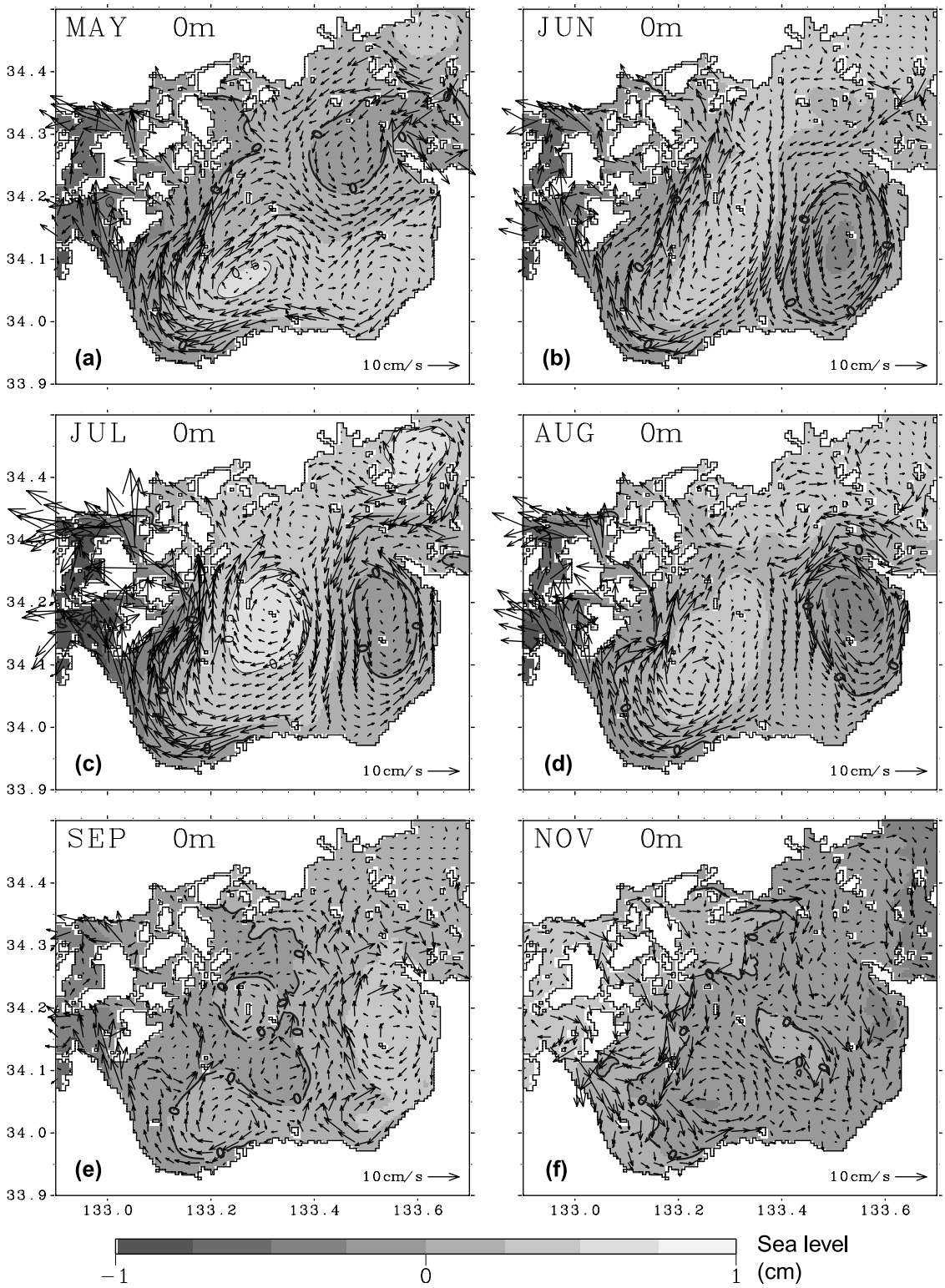

Figure 17. Horizontal distribution of residual current at the surface layer from the calculations without tide. Sea level distributions are also shown as a reference.

Strait and the Hiuchi-Nada. The other is an anticlockwise eddy in the eastern part, related to cold and dense bottom waters. The magnitude of the two eddies is ~10 cm/s.

[49] The average wind speed in the Hiuchi-Nada during the summer is around 2 m/s. The wind-driven current is very weak and is limited to the surface layer. It is difficult to identify the difference in the current distribution at 5 m depth from the calculations with and without wind (Figure 18). Therefore the existence of the two eddies in the bay in the summer is not affected by the wind. On the

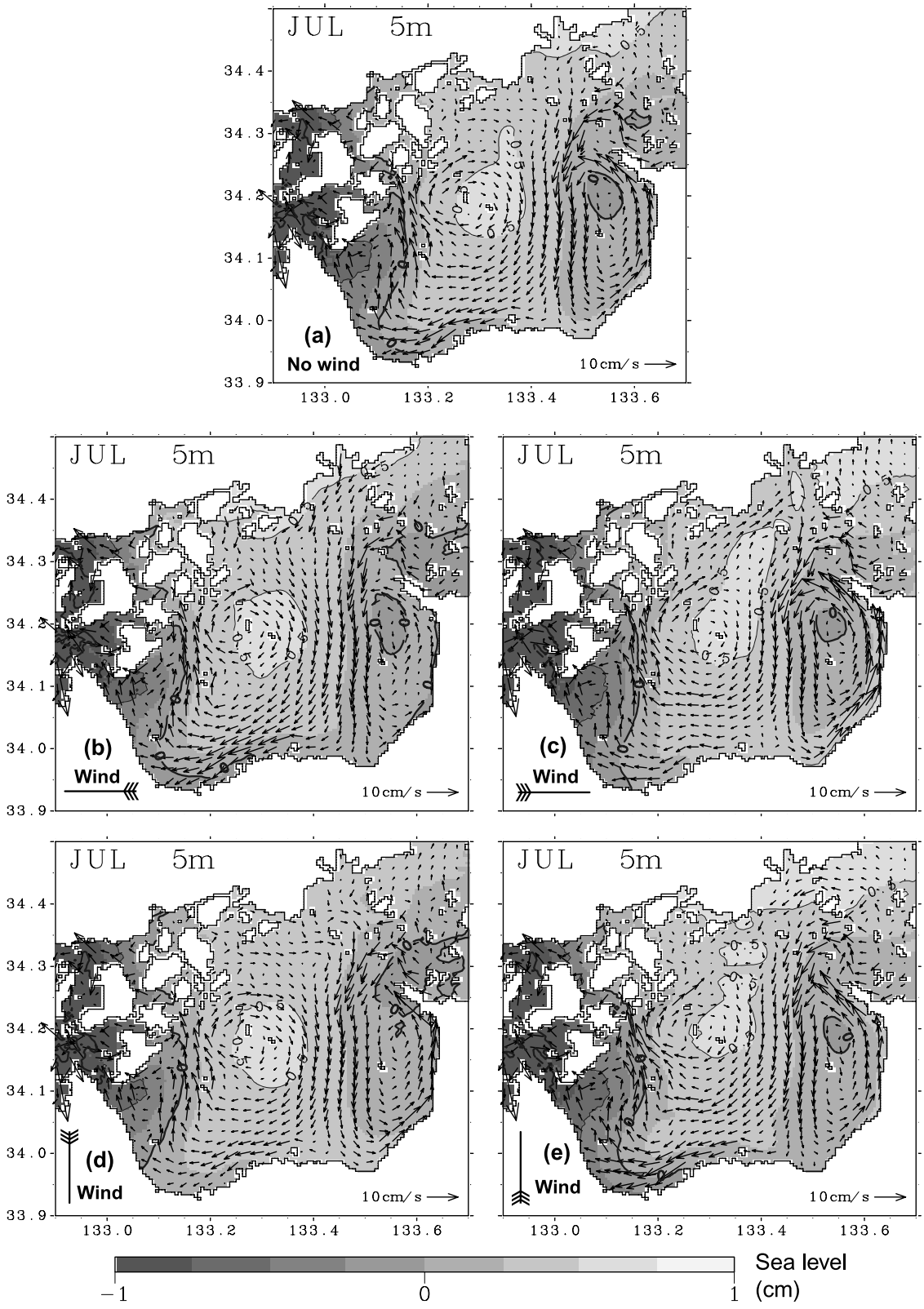

Figure 18. Residual current at 5 m in July, from the calculation (a) without wind, and with (b) east wind, (c) west wind, (d) north wind, and (e) south wind. Sea level distributions are also shown as a reference.

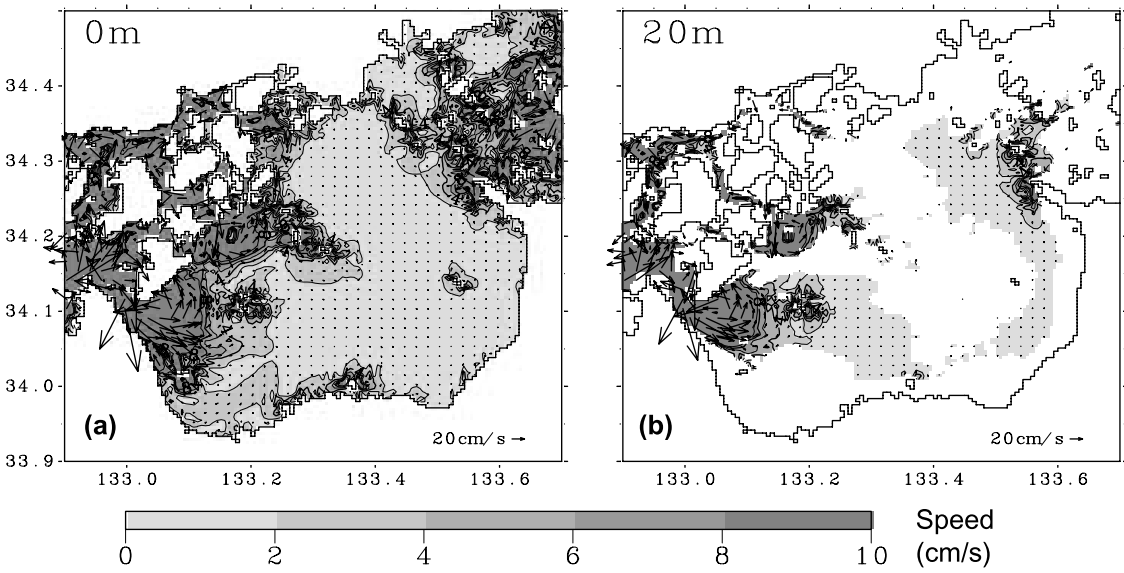

Figure 19. Horizontal distribution of tide-induced residual current at 0 and 20 m. The magnitude of the current is presented by dark tone.

other hand, tide-induced residual currents are restricted to the close vicinity of the Kurushima Strait and Bisan Strait. This component also does not affect the existence of the two eddies because the two eddies are located inside the bay.

[50] As a method to obtain the density-driven current, we adopted the robust diagnostic model. Another method could be geostrophic computation, which is simpler than the diagnostic calculation. There are two reasons why we did not use the geostrophic computation. Dynamically, in addition to the geostrophic balance, the internal friction also plays an important role in the density-driven current in a tide-dominant coastal area. The internal friction could alter the vertical structure of the geostrophic current. Technically, the geostrophic computation can obtain only the current component normal to the section of two hydrographic stations and is difficult to represent the horizontal distribution of the current in a bay. If the two hydrographic stations are across the flow direction, the geostrophic computation can produce the current. However, if the two hydrographic stations are along the flow direction, the geostrophic computation cannot produce the current. In our application, the hydrographic stations are not designed to be across the two eddies. Consequently, the purely geostrophic computation cannot produce the two eddies (not shown here).

[51] Usually, we cannot correctly predict the current pattern in a bay before the hydrographic survey and also cannot assure that the hydrographic stations are across the major currents in a bay. Therefore, although the geostrophic balance is an important dynamic in the coastal areas, the geostrophic computation is not a good method to produce the horizontal distribution of residual current in a bay.

[52] The robust diagnostic model is a useful tool to obtain the density-driven current from the results of hydrographic survey. Careful preparations of input density data are important to the diagnostic model. This can be achieved by rapid completion of hydrographic surveys over a wide coverage, which helps to reduce the inconsistency of input density data. Another important factor while applying robust diagnostic models to coastal waters is the treatment of tidal mixing in the model. In this application, we related the eddy viscosity/diffusivity to the tidal current. In the two straits where the tidal currents are stronger than 1 m/s, large vertical ($0.01\sim0.1$ m^2/s) and horizontal ($10\sim100$ m^2/s) eddy diffusivities are obtained (Figure 7). In the eastern part of bay where the tidal current is weaker than 0.1 m/s, small vertical ($\sim10^{-5}$ m^2/s) and horizontal (~0.1 m^2/s) eddy diffusivities are obtained. In the vertical, relatively large vertical eddy diffusivity is obtained near the bottom (Figure 7c). As shown in section 7, the distribution of eddy viscosity/diffusivity influences strongly on the intensity of calculated currents.

[53] From passive tracer experiments, we obtain different intrusion routes for waters from the Kurushima Strait and from the Bisan Strait into the Hiuchi-Nada. The water from the Kurushima Strait intrudes through the middle and bottom layers, while the water from the Bisan Strait intrudes through the surface layer. In Figure 21, we also show that water in the Hiuchi-Nada may enter the Kurushima Strait through the surface layer and move into the Bisan Strait through the bottom layer, which can be considered as compensatory effects to the intrusion of water from the two straits. This result can be inferred easily from current fields (Figure 10) and has been confirmed by additional calculations in which passive tracers have been released in the Hiuchi-Nada.

[54] The anticlockwise eddy in the eastern part of Hiuchi-Nada traps most of the tracer from the Bisan Strait and maintains it along the outer edge of the eddy, preventing the tracer from reaching the center of the eddy (Figure 14). This indicates that the anticlockwise eddy has no water exchange between its center and its outer edges, and therefore allows the development of oxygen-deficient waters in the central part of the eddy. However, the extent to which this horizontal isolation contributes to the formation of oxygen-

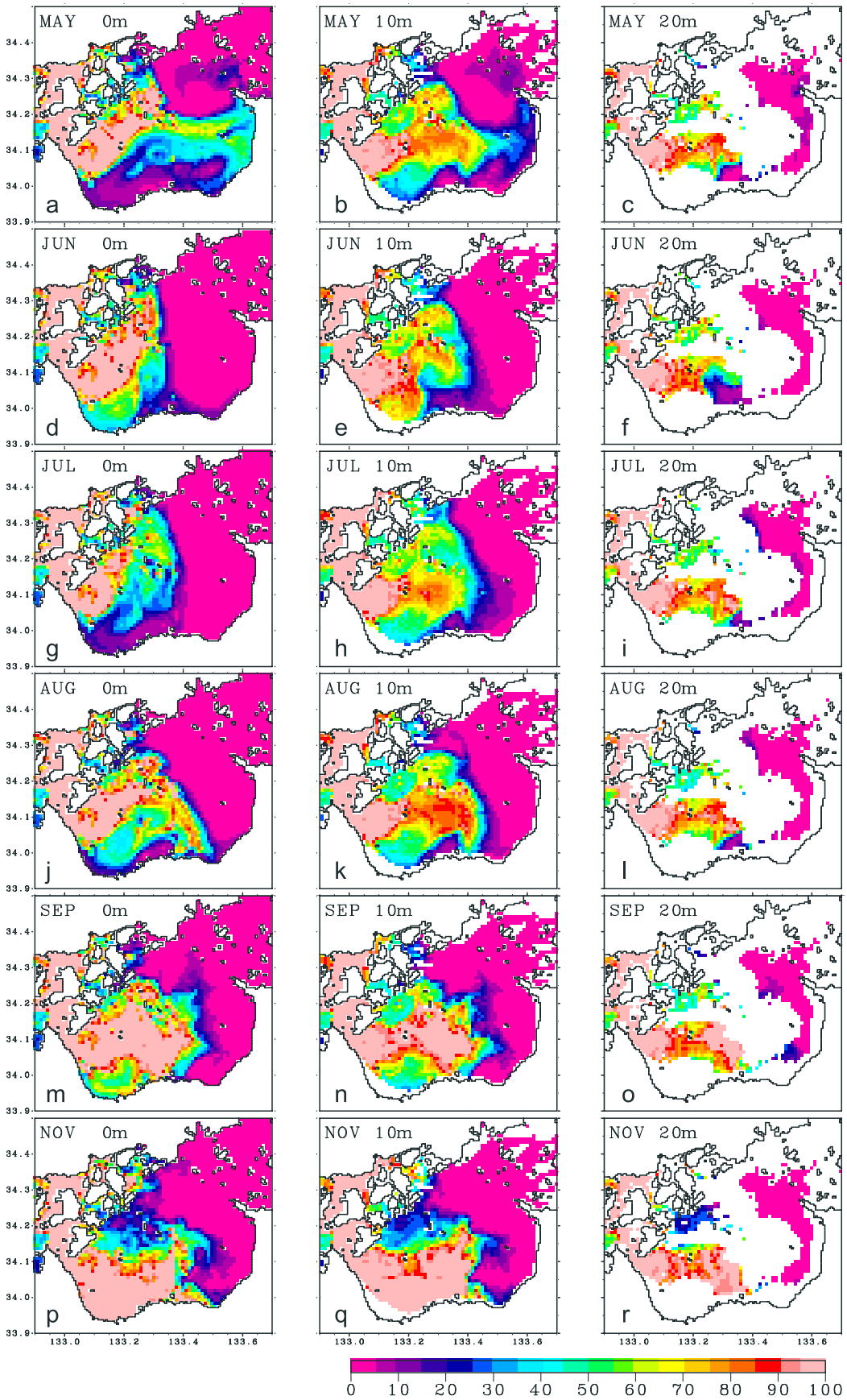

Figure 20. Horizontal distribution of tracer concentration at 0, 10, and 20 m, 30 days after being released in the Kurushima Strait, from the calculations including tide-induced residual current.

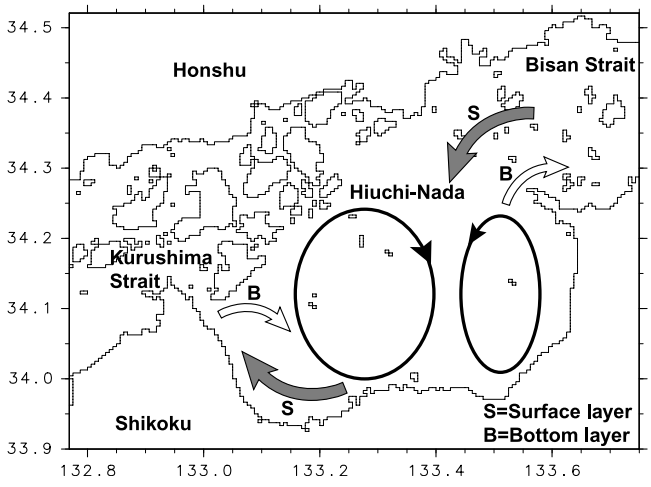

Figure 21. Schematic of circulation pattern in the Hiuchi-Nada in the summer and intrusion routes of passive tracer between the Hiuchi-Nada and Kurushima Strait and between the Hiuchi-Nada and Bisan Strait. Arrows denoted by an "S" indicate the intrusion in the surface layer. Arrows denoted by a "B" indicate the intrusion in the bottom layer referred to the local depth of two straits.

deficient water mass is still unknown and should be studied in the future with an ecosystem model.

[55] **Acknowledgments.** This research was supported by Grant-in-Aid for Scientific Research (A) from Japan Society for Promotion of Science (grant 12308027). Discussions with A. Kaneda and Y. Hayami were very helpful in planning observations. We appreciate Arnoldo Valle-Levinson and Andres Tejada-Martinez for their valuable suggestions on the manuscript and the reviewers whose comments helped to improve the manuscript. This paper was written while X. Guo was visiting the Center for Coastal Physical Oceanography at Old Dominion University. He thanks support from Ministry of Education, Culture, Sports, Science and Technology, Japan.

References

Beckmann, A., and D. Haidvogel (1993), Numerical simulation of flow around a tall isolated seamount, *J. Phys. Oceanogr.*, *23*, 1736–1753.

Bisagni, J. J. (1999), mates of vertical heat flux and stratification from southern Georges Bank, model descriptions and results, winter-summer 1995, *Cont. Shelf Res.*, *19*, 1065–1086.

Blumberg, A. F., and G. L. Mellor (1987), A description of a three-dimensional coastal ocean circulation model, in *Three-Dimensional Coastal Ocean Models*, *Coastal Estuarine Stud.*, vol. 4, edited by N. Heaps, pp. 1–16, AGU, Washington, D. C.

Burchard, H., O. Petersen, and T. P. Rippeth (1998), Comparing the performance of the Mellor-Yamada and the k-ε two-equation turbulence models, *J. Geophys. Res.*, *103*, 10,543–10,554.

Fujio, S., and N. Imasato (1991), Diagnostic calculation for circulation and water mass movement in the deep Pacific, *J. Geophys. Res.*, *96*, 10,756–10,774.

Fujiwara, T., and T. Higo (1986), Wind-induced current and mass transport in the Seto Inland Sea (in Japanese), *Bull. Coastal Oceanogr.*, *23*, 109–119.

Garrett, C. J. R., and J. W. Loder (1981), Dynamical aspects of shallow sea fronts, *Philos. Trans. R. Soc. London, Ser. A*, *302*, 563–581.

Guo, X., and T. Yanagi (1996), Seasonal variation of residual current in Tokyo Bay, Japan: Diagnostic numerical experiments, *J. Oceanogr.*, *52*, 597–616.

Harai, K., X. Guo, and H. Takeoka (2001), A tide model for Seto Inland Sea, Japan (II), paper presented at 2001 Fall Meeting, Oceanogr. Soc. of Jpn., Shimizu, Japan.

Hayami, K., and S. Unoki (1970), Exchange of seawater and diffusion of substance in the Seto Inland Sea (in Japanese), paper presented at 17th Conference on Coastal Engineering in Japan, Jpn. Soc. of Civ. Eng., Niigata, Japan.

Hill, A. E. (1996), Spin-down and the dynamics of dense pool gyres in shallow seas, *J. Mar. Res.*, *54*, 471–486.

Hill, A. E., J. Brown, and L. Fernand (1997), The summer gyre in the western Irish Sea: Shelf sea paradigms and management implications, *Estuarine Coastal Shelf Sci.*, *44*, Suppl. A, 83–95.

Holland, W. R., and A. D. Hirschman (1972), A numerical calculation of the circulation in the North Atlantic Ocean, *J. Phys. Oceanogr.*, *2*, 336–354.

Ishizaki, H., and M. Saito (1978), On the evaporation amount in the Seto Inland Sea (in Japanese), *Bull. Coastal Oceanogr.*, *16*, 11–20.

Lu, Y., R. G. Lueck, and D. Huang (2000), Turbulence characteristics in a tidal channel, *J. Phys. Oceanogr.*, *30*, 855–867.

Mellor, G. L. (1998), User's guide for a three-dimensional, primitive equation, numerical ocean model, report, 41 pp., Program in Atmospheric and Oceanic Sciences, Princeton University, Princeton, N. J.

Mellor, G. L., and T. Yamada (1982), Development of a turbulence closure model for geophysical fluid problems, *Rev. Geophys.*, *20*, 851–875.

Mellor, G. L., T. Ezer, and L.-Y. Oey (1994), The pressure gradient conundrum of sigma coordinate ocean models, *J. Atmos. Oceanic Technol.*, *11*, 1126–1134.

Mellor, G. L., Y. L.-Oey, and T. Ezer (1998), Sigma coordinate pressure gradient errors and the seamount problem, *J. Atmos. Oceanic Technol.*, *15*, 1122–1131.

Murakami, M., Y. Oonishi, and H. Kunishi (1985), A numerical simulation of the distribution of water temperature and salinity in the Seto Inland Sea, *J. Oceanogr. Soc. Jpn.*, *41*, 213–224.

Ochi, T., and H. Takeoka (1986), The anoxic water mass in Hiuch-Nada: 1. Distribution of the anoxic water mass, *J. Oceanogr. Soc. Jpn.*, *42*, 1–11.

Sarkisyan, A. S., and V. F. Ivanov (1971), The combined effect of baroclinicity and bottom relief as an important factor in the dynamics of ocean current, *Izv. Acad. Sci. USSR Atmos. Oceanic Phys., Engl. Transl.*, *1*, 173–188.

Sarmiento, J. L., and K. Bryan (1982), An ocean transport model for the North Atlantic, *J. Geophys. Res.*, *87*, 394–408.

Simpson, J. H., and J. R. Hunter (1974), Fronts in the Irish Sea, *Nature*, *250*, 404–406.

Simpson, J. H., D. G. Hughes, and N. C. G. Morris (1977), The relation of seasonal stratification to tidal mixing on the continental shelf, in *Deep Sea Res.*, *24*, Suppl., 327–340.

Simpson, J. H., W. R. Crawford, T. P. Rippeth, A. R. Campbell, and J. V. S. Cheok (1996), The vertical structure of turbulent dissipation in shelf seas, *J. Phys. Oceanogr.*, *26*, 1579–1590.

Stacey, M. T., S. G. Monismith, and J. R. Burau (1999), Observations of turbulence in a partially stratified estuary, *J. Phys. Oceanogr.*, *29*, 1950–1970.

Takeoka, H. (1985a), Density stratification in the Seto Inland Sea (in Japanese), *Mar. Sci. Mon.*, *60*, 145–152.

Takeoka, H. (1985b), Hiuchi-Nada (in Japanese), in *Coastal Oceanography of Japanese Islands*, edited by Coastal Oceanography Research Committee, Oceanographical Society of Japan, pp. 694–698, Tokai Univ. Press, Tokyo.

Takeoka, H. (1990), Criterion of tidal fronts around narrow straits, *Cont. Shelf Res.*, *10*, 605–613.

Takeoka, H. (2002), Progress in Seto Inland Sea research, *J. Oceanogr.*, *58*, 93–107.

Takeoka, H., Y. Ohno, and N. Inahata (1991), Roles of horizontal processes in the formation of density stratification in Hiuchi-Nada, *J. Oceanogr. Soc. Jpn.*, *47*, 33–44.

Tawara, S. (1986), Studies on the characteristics of oceanographic condition in relation to fishing condition in the shallow coastal waters (in Japanese), *J. Shimonoseki Univ. Fish.*, *34*, 1–103.

Wijesekera, H. W., J. S. Allen, and P. A. Newberger (2003), Modeling study of turbulent mixing over the continental shelf: Comparison of turbulent closure schemes, *J. Geophys. Res.*, *108*(C3), 3103, doi:10.1029/2001JC001234.

Yanagi, T., and H. Higuchi (1981), Tide and tidal current in the Seto Inland Sea (in Japanese), paper presented at 28th Conference on Coastal Engineering in Japan, Jpn. Soc. of Civ. Eng., Kochi, Japan.

Yanagi, T., and S. Okada (1993), Tidal fronts in the Seto Inland Sea (in Japanese), *Mem. Fac. Eng. Ehime Univ.*, *12*, 337–343.

Yanagi, T., and S. Takahashi (1993), Seasonal variation of circulations in the East China Sea and the Yellow Sea, *J. Oceanogr.*, *49*, 503–520.

Yanagi, T., and K. Yoshikawa (1987), Tidal fronts in Hiuchi Nada and Osaka Bay (in Japanese), *Bull. Jpn. Soc. Fish. Oceanogr.*, *51*, 115–119.

A. Futamura, Graduate School of Science and Engineering, Ehime University, Matsuyama 790-8577, Japan.

X. Guo and H. Takeoka, Center for Marine Environmental Studies, Ehime University, 2-5 Bunkyo-Cho, Matsuyama 790-8577, Japan. (guoxinyu@dpc.ehime-u.ac.jp)